Available online at www.sciencedirect.com
ScienceDirect
Journal of Volcanology and Geothermal Research 178 (2008) 416–453
Journal of volcanology and geothermal research
www.elsevier.com/locate/jvolgeores

Impact of explosive eruption scenarios at Vesuvius

G. Zuccaro [a,*], F. Cacace [a], R.J.S. Spence [b], P.J. Baxter [c]

[a] *Study Centre PLINIVS–LUPT, University of Naples "Federico II", via Toledo, 402-I 80122, Naples, Italy*
[b] *Cambridge Architectural Research Ltd., 25 Gwydir Street, 6, Cambridge, CB1 2LG, UK*
[c] *Institute of Public Health, University of Cambridge, Robinson Way, Cambridge CB2 2SR, UK*

Received 16 June 2007; accepted 3 January 2008
Available online 29 January 2008

Abstract

In the paper the first attempt at the definition of a model to assess the impact of a range of different volcanic hazards on the building structures is presented. This theoretical approach has been achieved within the activities of the EXPLORIS Project supported by the EU. A time history for Sub-Plinian I eruptive scenario of the Vesuvius is assumed by taking advantage of interpretation of historical reports of volcanic crises of the past [Carafa, G. 1632. In opusculum de novissima Vesuvij conflagratione, epistola isagogica, 2[a] ed. Napoli, Naples; Mascolo, G.B., 1634. De incendio Vesuvii excitato xvij. Kal. Ianuar. anno trigesimo primo sæculi Decimiseptimi libri X. Cum Chronologia superiorum incendiorum; & Ephemeride ultimi. Napoli; Varrone, S., 1634. Vesuviani incendii historiae libri tres. Napoli], numerical simulations [Neri, A., Esposti Ongaro, T., Macedonio, G., Gidaspow, D., 2003. Multiparticle simulation of collapsing volcanic columns and pyroclastic flows. J. Geophys. Res. Lett. 108, 2202. doi:10.1029/2001 JB000508; Macedonio, G., Costa, A., Longo, A., 2005. HAZMAP: a computer model for volcanic ash fallout and assessment of subsequent hazard. Comput. Geosci. 31,837–845; Costa, A., Macedonio, G., Folch, A., 2006. A three-dimensional Eulerian model for transport and deposition of volcanic ashes. Earth Planet. Sci. Lett. 241,634–647] and experts' elicitations [Aspinall, W.P., 2006. Structured elicitation of expert judgment for probabilistic hazard and risk assessment in volcanic eruptions. In: Mader, H.M. Coles, S.G. Connor, C.B. Connor, L.J. (Eds), Statistics in Volcanology. Geological Society of London on behalf of IAVCEI, pp.15–30; Woo, G., 1999. The Mathematics of Natural Catastrophes. Imperial College Press, London] from which the impact on the building structures is derived. This is achieved by an original definition of vulnerability functions for multi-hazard input and a dynamic cumulative damage model. Factors affecting the variability of the final scenario are highlighted. The results show the high sensitivity of hazard combinations in time and space distribution and address how to mitigate building vulnerability to subsequent eruptive phenomena [Baxter, P., Spence, R., Zuccaro, G., 2008-this issue. Risk mitigation and emergency measures at Vesuvius].

The first part of the work describes the numerical modelling and the methodology adopted to evaluate the resistance of buildings under the combined action of volcanic phenomena. Those considered here for this multi-hazard approach are limited to the following: earthquakes, pyroclastic flows and ash falls. Because of the lack of a systematic and extensive database of building damages observed after eruptions of such intensity of the past, approaches to this work must take a hybrid form of stochastic and deterministic analyses, taking into account written histories of volcanic eruptions and expertise from field geologists to build up a semi-deterministic model of the possible combinations of the above hazards that are situated both in time and space. Once a range of possible scenarios has been determined, a full stochastic method can be applied to find a sub-set of permutations and combinations of possible effects. This preliminary study of identification of the possible combination of the phenomena, subdividing them into those which are discrete and those which are continuous in time and space, enables consideration the vulnerability functions of the combinations to be feasible.

In previous works [Spence, R., Brichieri-Colombi, N., Holdsworth, F., Baxter, P., Zuccaro, G., 2004a. Vesuvius: building vulnerability and human casualty estimation for a pyroclastic flow (25 pages). J. Volcanol. Geotherm. Res. 133, 321–343. ISSN 0377-0273; Spence, R., Zuccaro, G., Petrazzuoli, S., Baxter, P.J., 2004b. The resistance of buildings to pyroclastic flows: theoretical and experimental studies in relation to Vesuvius, ASCE Nat. Hazards Rev. 5, 48–50. ISSN 1527–6988; Spence, R., Kelman, I., Petrazzuoli, S., Zuccaro, G., 2005. Residential Buildings and Occupant Vulnerability to Tephra Fall. Nat. Hazards Earth Syst. Sci. vol. 5. European Geosciences Union, pp.1–18; Baxter, P.J., Cole, P.D., Spence, R., Zuccaro, G., Boyd, R., Neri, A., 2005. The impacts of pyroclastic density currents on buildings during the eruption of the Soufrière hills volcano, Montserrat. Bull. Volcanol. vol. 67,292–313] the authors investigated, by means of experimental and analytical methods, the limiting resistance of masonry and reinforced concrete buildings assuming each action separately. In this work the first attempt to estimate the response of the buildings to the volcanic seismic action or to the lateral dynamic pressure due to pyroclastic flow combined with an extra vertical

* Corresponding author.
E-mail address: zuccaro@unina.it (G. Zuccaro).

doi:10.1016/j.jvolgeores.2008.01.005

load on the roof due to ash fall is performed. The results show that up to a certain limit of ash fall deposit, the increment of structure weight increases the resistance of a building to pyroclastic flow action while it reduces its seismic resistance. In particular the collapse of the top storey of R.C. buildings having large roofs could occur by accumulation of ash and a strong earthquake. Seismic and pyroclastic flow vulnerability of tall R.C. and masonry buildings with rigid floors is less sensitive to ash fall load combination. The model allows any sequence of events (earthquake, ash fall, pyroclastic flow) to be assumed and evaluates the spatial distribution of the cumulative impact at a given time. Single impact scenarios have been derived and mapped on a suitable grid into which the territory around Vesuvius has been subdivided. The buildings have been classified according to the constructional characteristics that mostly affect their response under the action of the phenomena; hence the vulnerability distribution of the buildings are assigned to each cell of the grid and by taking advantage from the combined vulnerability functions the impact is derived at time *t*.

In the paper the following impact simulations are presented:

- single cases of selected seismic sequence during the unrest phase (Sub-Plinian I)
- ash fall damage distribution compatible to a Sub-Plinian I eruption
- pyroclastic flow cumulative damage scenarios for selected cases (Sub-Plinian I).

The model also allows either Monte Carlo simulation to evaluate the most probable final scenario or maximisation of some parameter sensitive to Civil Protection preparedness. The analysis of the results derived for a Sub-Plinian I-like eruption has shown the importance of the seismic intensities released during the unrest phase that could interfere with the evacuation of the area and the huge number of partial collapses (roofs) due to ash fall.

Keywords: Sub-Plinian I eruption; cumulative damage; impact scenarios; probabilistic model

1. Introduction

The evaluation of the possible effects due to a volcanic eruption in an urbanised region, such as the realization of a credible impact scenario, represents a very complex problem and a quite unexplored field of interest. The damage impact scenario in fact can be quite different depending on the type of eruption, both because of the development over time of the different phenomena that characterize it and because of the urbanistic and typological–structural characteristics of the buildings and of the infrastructures in the study area.

A volcanic eruption is characterized by a series of successive physical phenomena, so the damage impact due to a volcanic eruption depends upon several disastrous events, different even though tightly connected, each of which contributes in different way to the final scenario.

Within the EXPLORIS Project three of these phenomena have been studied: earthquakes (EQ), ash falls (AF) and pyroclastic flows (PF).

The impact on building structures deriving from the combination of different volcanic actions has been rarely studied. Extensive statistical databases on such damage are not available from previous cases, except some information that could be derived from recent eruptions around the world (Rabaul, Montserrat, etc.) and by interpreting historical reports of volcanic crises of the past. In the EXPLORIS Project, some historic manuscripts describing the 1631 eruption have been translated from Latin and ancient Italian, and these have supplied useful information to validate the assumptions and the results of this work.

The goal is to develop a dynamic model, here presented, that simulates the whole eruptive process, from the first precursory seismic events up to the final pyroclastic flows, evaluating at every step of the process, the damage accumulated on the buildings and the distribution of the damage on the territory.

It is considered, in fact, that the sequence of events during the eruption causes a progressive diminution of the resistance characteristics of the buildings, depending on the evolution of the damaging process.

Therefore an important starting point is represented by the event tree (ET) (Aspinall et al. 2008-this issue) developed in EXPLORIS (Fig. 1) that estimates the probabilities of occurrence for each of the possible eruptive scenarios, or rather of the possible typologies of eruptive process.

The model for damage evaluation has been tested for a "Sub-Plinian I" style of eruption, with the creation of maps that describe the impact of the eruption on the region and the evaluations of the losses, either in terms of building damage (number of collapses, heavy damaged etc.) or in terms of casualties (people killed, people seriously injured and homeless).

The model has been tested also for a violent Strombolian type eruption, for which only preliminary results are reported elsewhere in this volume (Baxter et al., 2008-this issue).

2. Event definition

The combination of the three volcanic phenomena can increase damage on buildings by comparison with the effects of each one acting separately. The real impact resulting from the load combination is dependant on the possible eruptive scenario assumed. The dynamic evolution of the eruption will impose the real loading combination at a specific time in the evolution of the eruptive event. Therefore, in order to simplify such a complex task and considering the great uncertainty in the definition of the load history derived from different eruptive

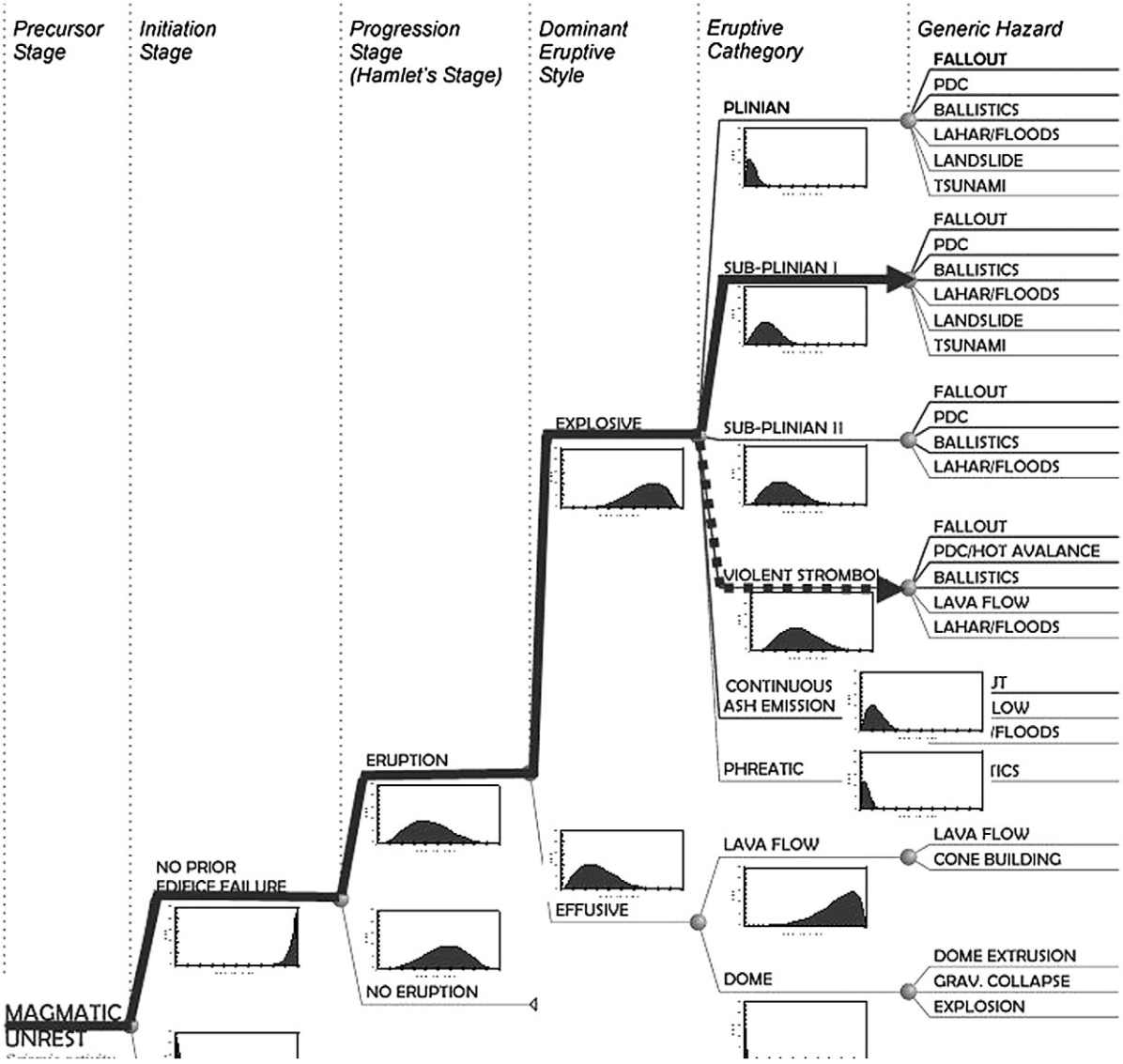

Fig. 1. The explosive branch of the EXPLORIS event tree — example of Vesuvius (Aspinall et al., 2008-this issue).

scenarios identified by the event tree sets in this project, some basic considerations and simple preliminary assumptions have been made.

First, in order to evaluate the possibility of simultaneous events, we should distinguish them as either *continuous*: AF which tends to occur throughout an eruption, or *discrete*: EQs which last for seconds or PFs each pulse of which can last a few minutes.

Secondly, the events have a different probability distribution in space. For impact purposes, AF and EQ can be assumed to have an almost uniform distribution in the most affected zones so that a large population of buildings is affected. The PFs are instead less uniformly distributed over space; nevertheless, they can be numerous so that a considerable number of buildings would be involved.

Third, simple assumptions about the time distributions of the events expected, based on the eruptive scenario assumed (event tree), can be made. Hence impossible or highly improbable combinations can be eliminated.

Moreover, this approach allows the tracing of the impact scenario's evolution through time and over space, providing important information to authorities responding to the disaster.

In the following a sample of possible preliminary assumptions based on a Sub-Plinian I scenario at Vesuvius, akin to the 1631 eruption is reported:

EQ:
- Before the eruption, 2–5 discrete events could occur with the biggest likely to be in the range of intensity VII–VIII of the European Macroseismic Scale (EMS '98).
- During the eruption, a continuous seismic activity of low intensity (less than intensity V) is expected (tremors).
- In addition, some discrete, short events (20–40 s) are expected of low intensity (V–VI EMS) during the AF phase.
- The area influenced by EQ around Vesuvius is mainly the Red Zone of the Emergency Plan produced by the Italian Department of Civil Protection (Fig. 2) (Department of Civil Protection, 2001).

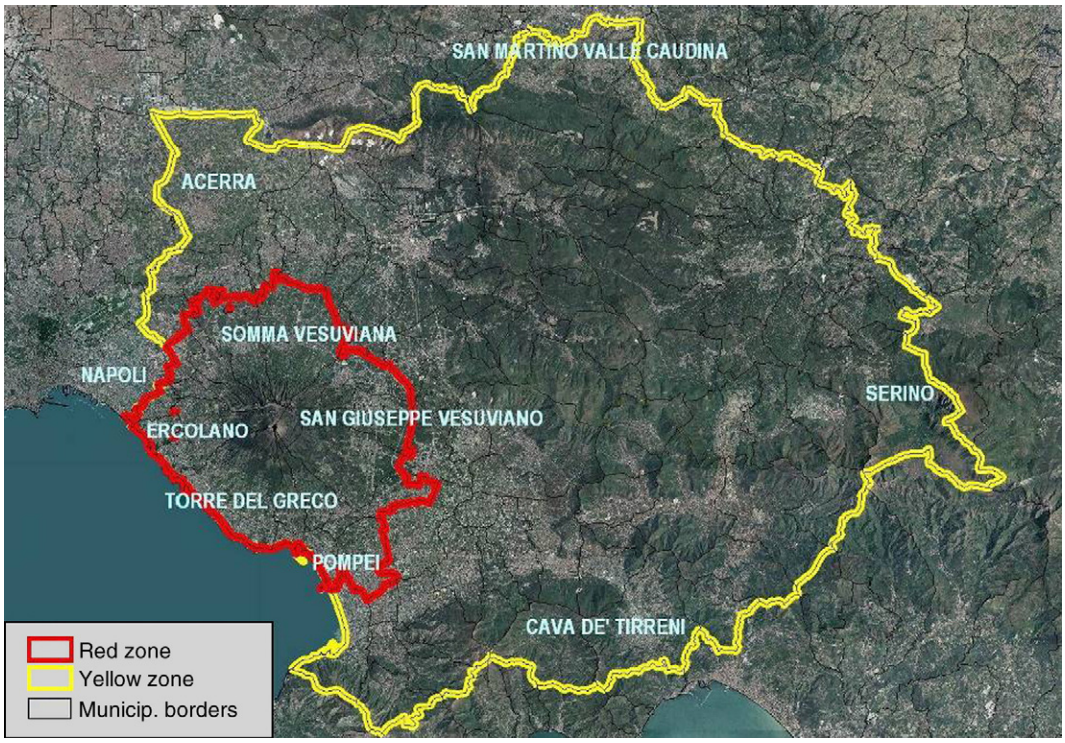

Fig. 2. The area influenced around Vesuvius is mainly the Red Zone of the Emergency Plan produced by the Italian Department of Civil Protection (2001) (Department of Civil Protection, 2001).

AF:
- During the eruption, it is continuous, starting from the onset of the eruption and gradually increasing the deposit and the consequent load on the roofs.
- The area influenced around Vesuvius is mainly the Red Zone, but then the Yellow Zone follows (Fig. 2).
- Soon after the eruption the wind in the stratosphere continues to disperse ash in the distal areas impacting the Yellow Zone.

PF:
- Approaching the end of AF phase and immediately afterwards a series of discrete PF events occurs having durations of 3–4 min each, randomly distributed in time during the last eruption phase. The spatial distribution is also random and the damaging impact front can be assumed to be from 150 to 500 m wide.
- The area influenced around Vesuvius is mainly the Red Zone.

2.1. Possible event combinations of Vesuvius

The final impact is strongly influenced by the event combination. Based on the considerations of the previous paragraph a possible event combination for the Sub-Plinian I eruption is here presented.

Before the eruption — Phase 1:

- The impact scenario in the Red Zone is determined by the EQs.
- The impacts are determined by using standard EQ vulnerability functions, shown in Section 4.1, and evaluating the cumulative damage due to the greater vulnerability of the buildings affected by any previous earthquake (EQ → EQ).

During the eruption — Phase 2:

- The impact scenario in the Red Zone is determined by AF occurring continuously with some EQs occurring randomly.
- The impacts in the Red Zone are given by:
  - The AF damage distribution that increases with time and that can increase the EQ damage, especially on the masonry buildings (AF → AF, EQ → AF).
  - The EQ damage distribution increases by possible AF deposit on roofs. This damage can also grow for a sequence of earthquakes of moderate energy (V–VI EMS) (AF → EQ, EQ → EQ).

After the AF — Phase 3:

- The scenario in the Red Zone is characterized by PFs occurring randomly.

Table 1
Sequence probability of the events

First↓ second→	EQ	PF	AF
EQ	High	High	High
PF	Moderate	Low	Low
AF	Moderate	High	High

Table 2
Seismic-building structures classification

Vertical structures	Horizontal structures				
	Poor rigidity	Poor technology	Medium rigidity	Medium high rigidity	High rigidity
	Vaults and/or wooden floor (without ties)	"SAP" floor	Vaults and/or wooden floor (without ties)	Iron beam floor	Reinforced concrete floor
Weak masonry Rubble masonry neglected (lavic stone, not squared tuff, etc.)	A_s	A_s	A_s	A_s	A_s
Medium quality Rubble masonry maintained (lavic stone, not squared tuff, etc.)	A_s	A_s	B_s	B_s	B_s
Good masonry Squared masonry (lavic stone, tuff etc.)	A_s	A_s	B_s	B_s	C_s
Framed structures (R.C. or steel)	–	B_s	–	–	D_s

- The impacts in the Red Zone are given by:
  - The PFs, discrete events randomly distributed over space. The standard damage distribution given by PF vulnerability functions, shown in Section 4.3, could be increased by the presence of damage caused by previous PF (rare) or previous EQ (likely), but could be reduced by the benefits (in this case) of AF on the roofs (PF → PF, EQ → PF, AF → PF).

After the eruption:

- The scenario in the Yellow Zone is given by AF.
- The impacts in the Yellow Zone are given by AF vulnerability functions, shown in Section 4.2.

2.2. Coincidence of events

The probability that a building is hit at same time by two or more events is worth considering only in the cases of AF+EQ and AF+PF. The cases of considerable EQ and PF simultaneously are assumed to have a very low probability since EQ and PF are both short-lived discrete events. Therefore, these cases and also the case of all three events at same time have been neglected.

2.3. Sequence of events

The probability that a building is hit by a sequence of different events with considerable consequences for its structural integrity is summarised in Table 1.

2.4. Structural response under combined actions

The final impact scenario can be examined by trying to parameterise the cumulative damage that the structure experiences from the possible sequence of events. The problem can be treated as a sort of progressive deterioration of the building's resistance characteristics that is essentially represented by the damage level. This requires the assumption of one damage scale as descriptor of the global structural damage of the different building classes.

The seismic damage scale has been then assumed as referring to describe also the damage level caused by the other phenomena (AF and PF). To this aim the non-structural elements (NSE) vulnerability (windows, doors, infill panels etc.) under the action of PF have been taken into account separately (and compatible with Spence et al., 2004b; Baxter et al., 2005); however the consequences on the structure of the NSE failure (fire, roof explosion, casualty etc.) has been considered in terms of seismic equivalent global damage and has affected the vulnerability curve evaluations of Section 4.3. Moreover the failure of NSE is a crucial factor for casualty estimation as reported in Baxter et al. (2005). For AF events, the damage levels considered are D4 and D5 only and they are assimilated to roof partially/totally collapsed;[1] in this case the building is considered "lost". No damage of lower level (D1–D3) is considered as directly caused by AF; rather it influences all damage levels due to the others phenomena (EQs, PFs) as described in Section 5 (Baxter et al., 2005).

Now assuming that in theory the structures can survive numerous moderate events when an "ideal elastic threshold" (conventional specially for masonry buildings) is not violated, and assuming that with reference to the damage levels of the EMS '98 (EMS, 1998) this corresponds to a damage level < D3 general assumptions confirmed by experience could be:

- Buildings can survive numerous events that cause damage level D2.
- When the building, because of some previous event or events reaches damage class D3, the structure is not in a

[1] This is because only vulnerability curves at limit state of collapse are available, as described in Section 4.2.

Fig. 3. Torre Annunziata: detail of the vulnerability building classes: A_s, B_s, C_s, D_s (EMS-98).

condition to survive another event comparable to the last event that caused D3 without being at least partially collapsed.

A model of cumulative damage due to sequence of events on the structures has been then calibrated and presented in Section 6.

3. Inventory of elements at risk at Vesuvius and GIS

The elements at risk considered in the analysis are the building structures and the population in the Vesuvian villages of the Red Zone and of the Yellow Zone. The inventory is derived either from the census data (1991–2001) of the Italian Institute of Statistic (ISTAT) or from specific collections of data in the field carried out in the last 10 years of research in the area (Baratta and Zuccaro, 1989; Zuccaro, 2000; Cherubini et al., 2002).

Specific survey forms containing all the information required for a complete characterization of the structures resistance have been prepared.

A Geographic Information System (GIS) of the factors influencing the building response for EQ, PF and AF has been set. The following list shows the main categories of data collected:

- Vertical structure
- Horizontal structure
- Age
- No. of storeys
- Roof typology
- Type and size of the openings.

On the basis of the data collected, characterizations of the building structures to the three different hazardous phenomena (EQ, AF, PF) are set up.

3.1. Seismic-building structures classification

From the combination of vertical and horizontal structure classifications a first assignment of the seismic-building structure classification is done (Table 2), (Fig. 3); then, through an original procedure that takes into account other constructive characteristics influencing the seismic response, the final EQ vulnerability class is assigned (Zuccaro, 2004; Zuccaro and Cacace, 2006).

3.2. Ash fall — roof classification

The roof vulnerability classification of Table 3 is based on the roof structural typologies surveyed in the region where this phenomenon is expected. In the Red Zone data on 19,000 buildings have been collected using a specific form. This set represents about 30% of the whole building population. From these data, a correlation relationship (Fig. 4) between seismic vulnerability and roof vulnerability class is derived. Applying this law it is possible to estimate the roof vulnerability distribution for the whole set of buildings.

Table 3
Ash fall — roof structural classification

Type	Description
A_r	Weak pitched wooden roof
B_r	Flat standard wooden roof
	Reinforced concrete flat roof — SAP type
	Weak steel and little vaults flat roof
$C1_r$	Flat R.C. roof older than 20 years
$C2_r$	Flat R.C. younger than 20 years
	Recent flat R.C. flat roof
D_r	Recent pitched R.C. roof
	Recent pitched steel roof

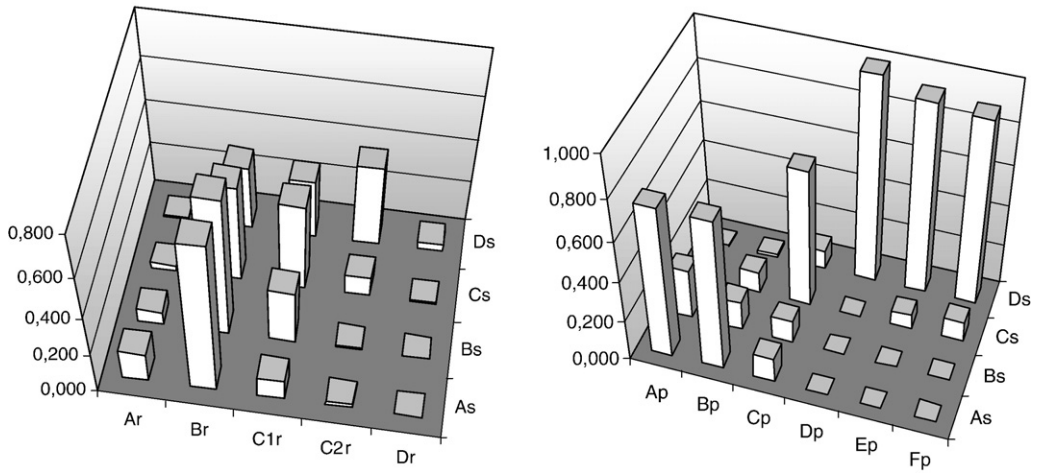

Fig. 4. Correlation between seismic vulnerability classes (A_s, B_s, C_s, D_s) and ash fall (A_r, B_r, C_r, D_r) and pyroclastic (A_p, B_p, C_p, D_p) vulnerability classes.

3.3. Pyroclastic flow — building structure classification

The structural classification to evaluate the vulnerability of the buildings under the action of the pyroclastic flows has been carried out by evaluating preliminarily the importance of some building structure elements, through simple numerical elaboration of R.C. and masonry structures models at limit state of collapse.

The prevalent typological characteristics influencing the structural response of the building under the pyroclastic flow action, apart from the intrinsic resistance characteristic of the structure as the geometry and the quality of the material, are:

– the weight of the building
– the height of the building
– the capacity of some crucial elements to resist at the lateral pressure.

Table 4
Pyroclastic flows — structural classification

Type	Description
A_p	Weak masonry buildings of 3–4 storeys with deformable floor. Weak or strong masonry buildings with more than 4 storeys.
B_p	Medium masonry buildings of 1–2 storeys with deformable floor. Strong masonry buildings of 3 or more storeys with rigid floor.
C_p	Strong masonry buildings of 1–2 storeys with rigid floor.
D_p	Non-aseismic R.C. buildings of more than 6 storeys (high).
E_p	Non-aseismic R.C. buildings of 4–6 storeys (medium).
F_p	Non-aseismic R.C. buildings of 1–3 storeys (low).

Table 5
Parameters considered to characterize masonry buildings in the Vesuvian villages

Building type	Wall thickness in average (cm)	Compressive rupture resistance (kg/cm^2)	Vertical load on the walls (tonnes per m length)	Inter-storey height (m)
Strong	Constant=60	Random (10–25)	Random (0–1.5)	3.5
Medium	Constant=50	Random (10–25)	Random (0–1.5)	3.5
Weak	Constant=40	Random (10–25)	Random (0–1.5)	3.5

3.4. Masonry structures

Two families of masonry structures have been considered:

– masonry buildings with rigid floors
– masonry buildings with deformable floors.

Within these two families of buildings, and increasing the number of storeys, three types of buildings have been analysed varying randomly the parameters chosen to evaluate the lateral resistance (i.e. thickness of the walls, quality of the materials etc., see Table 5) and three types of vulnerability classes are defined (A_p, B_p, C_p).

3.5. Reinforced concrete structures

The majority of the buildings in the Vesuvian area are not to conform to the seismic code.

The reinforced concrete typologies have been subdivided into three vulnerability classes (D_p, E_p, F_p) according to the number of storeys. Table 4 shows the six types and their description.

Also in this case it is possible to derive a correlation between seismic and pyroclastic vulnerability classes (Fig. 4).

These correlations are important since in calculating damage the memory of the cumulative damage of the building heritage is always referred to the inventory of the seismic-building typologies.

4. Vulnerability — general approach

The impact evaluation model of combined actions requires necessarily a probabilistic approach because of the wide range of uncertainties in the quantification of the loads, the mode of their application to the structures and the structural typology characteristics at an urban scale. However a purely stochastic

approach without any link to the physics of the problem could lead to false results.

Therefore, a hybrid approach has been followed in order to achieve the most reliable, although approximate, results. Three tools of investigation have been used:

- Numerical modelling.
- Loading tests.
- Probability distribution.

Firstly, each phenomenon has been studied separately and a refinement of previous vulnerability functions has been achieved. The necessity to harmonise the vulnerability distributions of each kind of event, in order to study the subsequent load combinations, has required a further effort in calibrating these curves in order to make the comparisons possible.

Moreover, the background knowledge of the impact of the three types of events considered is inhomogeneous. For example, the seismic impact in Campania region, is strongly supported by 25 years of studies, damage distribution surveys of the past tectonic events and consolidated vulnerability functions including damage probability matrices, fragility curves, and capacity curves (Braga et al., 1982; Baratta and Zuccaro, 1989; Di Pasquale and Orsini, 1997; Grimaz et al., 1997; Woo, 1999; Zuccaro et al., 1999; Zuccaro, 2004; Zuccaro and Cacace, 2007a). In comparison, the response of the structures to pyroclastic flow and ash fall loads is a fairly recent field of interest (Spence et al., 1997, 2004b, 2005; Pomonis et al., 1999; Zuccaro and Petrazzuoli, 2004a; Baxter et al., 2004; Baratta et al., 2004).

Therefore, to approach the definition of PF and AF vulnerability curves, a deterministic set of analyses on several samples of typical Vesuvian structures have been performed. By varying the geometrical and mechanical characteristics of the structures, a set of collapse limit load (CLL) ranges has been derived using a Monte Carlo simulation method. In addition, the AF vulnerability functions have been validated by a campaign of loading tests performed on typical flat-roofed structures chosen in the Vesuvian area.

The PF vulnerability functions (VF) derived in previous researches (Zuccaro, 2000; Spence et al., 2004b) have been refined. The horizontal load profile, assumed constant in the

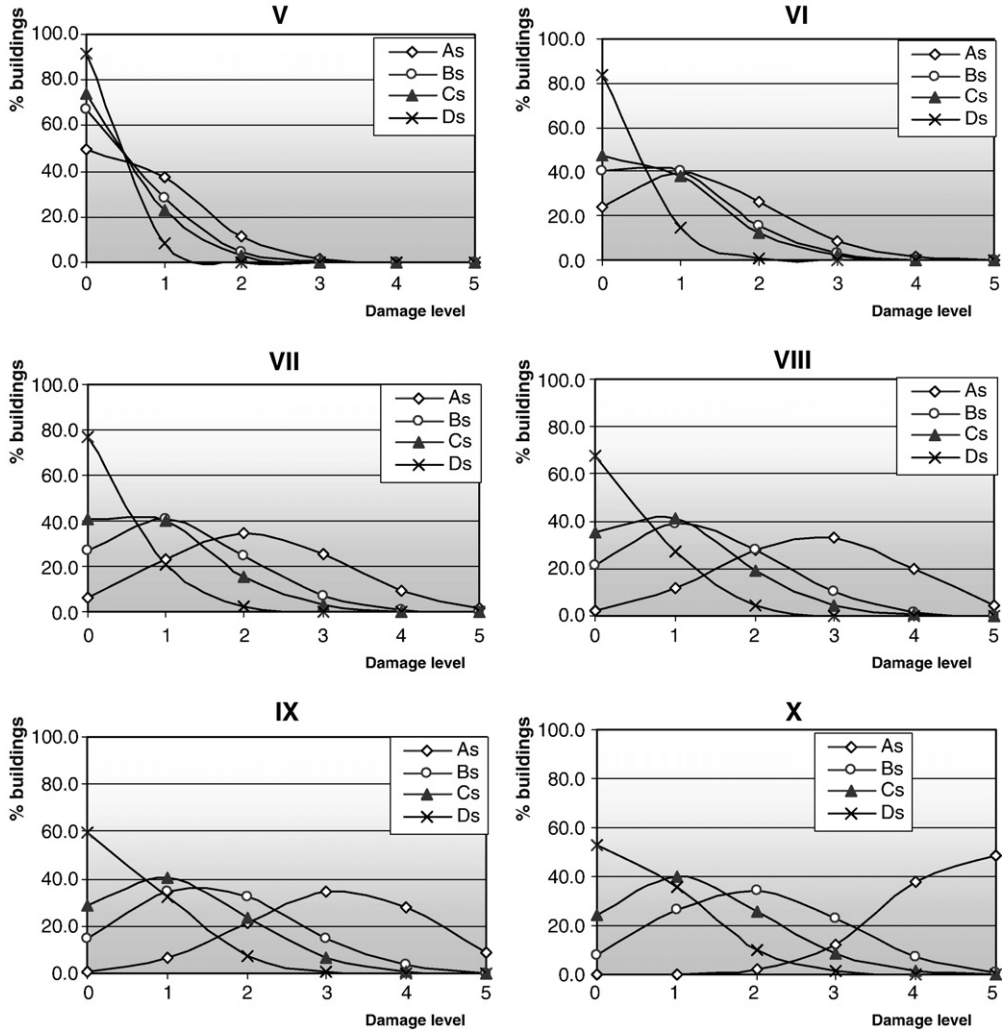

Fig. 5. Earthquake damage probability functions for different structural typologies.

previous analyses, has been now modelled by non-linear curves derived from new information on the density and velocity varying with height in the range 0–30 m. This has produced new CLL values that compared with the previous have not shown significant differences. Moreover, a new set of limit load analyses has been performed and a new set of CLL curves defined. These have been compared with results from some recent "push over" tests performed on reinforced concrete buildings in the Campi Flegrei area (Zuccaro and Petrazzuoli, 2004a) and with results from other "push over" tests found in the literature (Zuccaro and Petrazzuoli, 2004a). These comparisons have validated the curves defined.

Finally the minimum and the maximum values of the collapse loads computed for PF, have been assumed respectively as the 5th and 95th percentiles of collapse probability, and by means of the standard deviations of the Monte Carlo simulations a final set of vulnerability curves at the state of collapse having Gaussian Distribution has been derived for buildings with a given number of storeys.

These studies have refined the probability distribution of the highest damage class (D5) for different structural vulnerability classes. The damage distribution from D0 (no damage) to D5 (total collapse) is well-established in seismic vulnerability assessment (EMS '98) while the variations of damage for PF and AF are definitely more uncertain. Based on the results obtained in Zuccaro (2000), a first attempt for volcanic damage classification for AF and PF events has been achieved.

4.1. Earthquake vulnerability functions

Fig. 5 reports the damage probability curves recently calibrated for seismic events in Italy; the typologies A_s…D_s are based on the EMS '98 assumptions (Zuccaro, 2004).

The correlation between building type, damage and intensity expressed by the graphically-presented damage probability matrices (DPM) in Fig. 5 and calibrated for tectonic EQ may be assumed to be valid also for volcanic EQ. The main difference between volcanic and tectonic EQ are the shorter attenuation distance and the different magnitude/intensity relationship because of the shallow depth of the volcanic EQs. However these factors do not affect the building type damage distributions expressed by the DPM if the expectations of the EQ shaking are referred directly to intensity and the attenuation laws are calibrated in macroseismic intensity on specific local models (Department of Civil Protection, 2006).

These DPM have been compared with the damage distribution of the volcanic earthquake of Santa Venerina in Sicily on the Etna volcano. A good agreement was found (Zuccaro, 2000).

4.2. AF vulnerability functions

Ash fall vulnerability functions have been defined for several flat structure types by numerical simulations of roof behaviour at limit state of collapse. By varying the assumptions on the constraints end and on the material strength, lower and higher limits load have been derived for each roof type with reference to a single-span slab 5 m wide.

The limit additional load Q_{lim} has been determined considering the usual failure mechanism of horizontal structures characterized by the formation of three plastic hinges: two at the extremes and one in the middle of the span.

$$Q_{lim} = \alpha\beta M_u / l^2 - q_p \quad (1)$$

where:

l	the beam's length (m)
M_u	limit bending moment in the centre of the span, (kN m per unit of slab width)
q_p	permanent load (kN/m^2)
α	coefficient relating to constraints and reinforcements at the ends, ranging from 0 to 16, and depending on values of M_{uj} (limit bending moment at the ends) and M_u
β	factor representing the strength increment induced by non-structural layers as pavement, cement etc., ranging from 1.2 to 1.5.

These estimated values have been based upon dynamic tests (Spence et al., 2004b). By means of Eq. (1), the values of maximum and minimum mean resistance for each structural typology have been evaluated. Then, a normal probability distribution has been fitted in the range of the lower and upper bound and the cumulative probability functions have been derived (Fig. 6).

Loading tests up to the collapse limit have been performed on a sample of real roofs and the results have shown a good agreement with the theoretical curves shown above (Spence et al., 2004b).

4.3. PF vulnerability functions

A refinement has been made to limit state of collapse curves against horizontal dynamic pressures defined in a previous work (Zuccaro, 2000).

4.3.1. Masonry buildings

A systematic Limit State Analysis to evaluate the resistance of the masonry buildings to dilute horizontal PF currents has been performed.

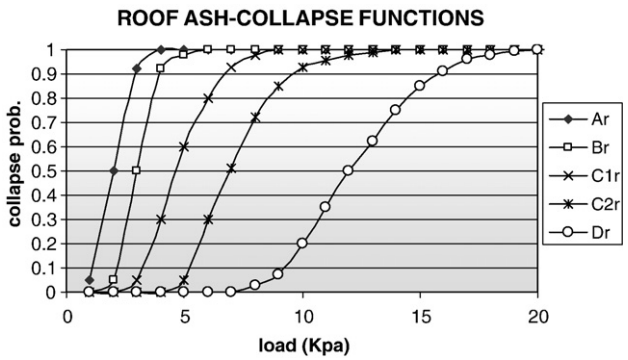

Fig. 6. Collapse probability functions for different roof typologies.

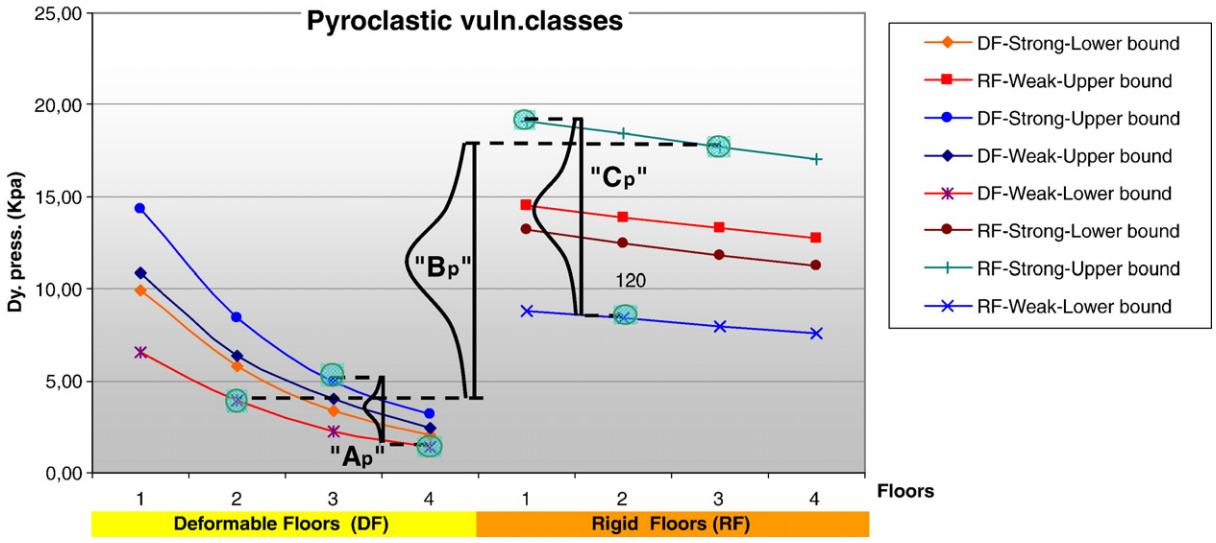

Fig. 7. Lower and upper bounds of the horizontal loads at the limit state of collapse derived for building types of different mechanical and geometrical characteristics. Identification of the vulnerability classes of Table 5 and their possible Gaussian probability distribution.

Since the response of the structures to horizontal load is strongly dependant on the rigidity of the floor, as well-known in seismic engineering, two families of structures have been considered: masonry buildings with *rigid floors* and masonry buildings with *deformable floors*.

Within these two families of buildings, and increasing the number of storeys, three types of buildings have been analysed: Strong, Medium and Weak by varying randomly the parameters considered according to different mechanical and geometrical characteristics (see Table 5).

The horizontal pressure limit (HPL) for each building type has been evaluated by varying the parameters of Table 5 in order to find the extreme values (upper and lower bounds) of the collapse limit load for buildings with a given number of storeys.

The results from the numerical simulation at the limit state of collapse are in Fig. 7.

Fig. 7 shows the curves obtained diagramming the upper and lower bounds of the horizontal limit load varying the parameters of Table 5 for each building type of assigned number of storeys. Three different vulnerability classes have been then identified for masonry buildings (A_p, B_p and C_p) according to the number of storeys as in the typological description of Table 5. The lower and the upper bounds of the curves of Fig. 7 represent respectively the 5th and the 95th percentiles of the collapse probability obtained by Monte Carlo (MC) simulations at the limit state of collapse on a simplified model. By means of standard deviation obtained from MC simulations a final set of vulnerability curves at the state of collapse having Gaussian Distribution has been derived for buildings with a given range of number of storeys.

4.3.2. PF damage probability functions

The collapse probability functions in Fig. 7 show the probability that a building is affected by a D5 damage (collapse). Starting from these functions it has been possible to assess compatible functions for damage levels from D1 to D4 (see for details Baxter et al., 2005); this has been done by observing the progressive damage of the building before the collapse and assigning a value of lateral pressure corresponding to each damage level, starting from non-structural damage and subsequently applying increasing pressure. The binomial distribution represents the best statistical fitting of the damage variation derived from the analysis described.

These binomial coefficients define the expected distribution of damage due to PF action for each combination of dynamic pressure and vulnerability classes, see Table 6(a).

By using the binomial coefficient formula it is possible to derive the values of the damage probability matrices (DPM) for each class of typology and for each lateral pressure value.

$$V_{khi} = \frac{5!}{k!(5-k)!} \cdot p_{hi}^{k}(1-p_{hi})^{5-k} \tag{2}$$

Where V_{khi} is the single vulnerability coefficient that represents the percentage of damage level k (k=0…5)) for each expected value i of dynamic pressure (DP) (i=1 kPa, 2 kPa,…, 14 kPa) and for each building typology for PF considered h (h=A_p,B_p,…, F_p).

In Fig. 8 a sample of PF–DPM is reported.

Table 6

Class	Dynamic flow pressure (kPa)								
	2	3	4	5	6	8	10	12	14
(a) Binomial coefficients for masonry under pyroclastic flow action									
A_p	0.082	0.176	0.657	0.8	0.885	0.979	1	1	1
B_p	0.082	0.102	0.129	0.241	0.404	0.842	0.95	1	1
C_p	0.081	0.102	0.129	0.183	0.248	0.36	0.473	0.749	0.933
(b) Binomial coefficients for R.C. building under pyroclastic flow action									
D_p	0.082	0.132	0.56	0.885	0.978	1	1	1	1
E_p	0.082	0.132	0.409	0.751	0.961	1	1	1	1
F_p	0.082	0.132	0.249	0.411	0.576	0.765	0.935	0.967	0.979

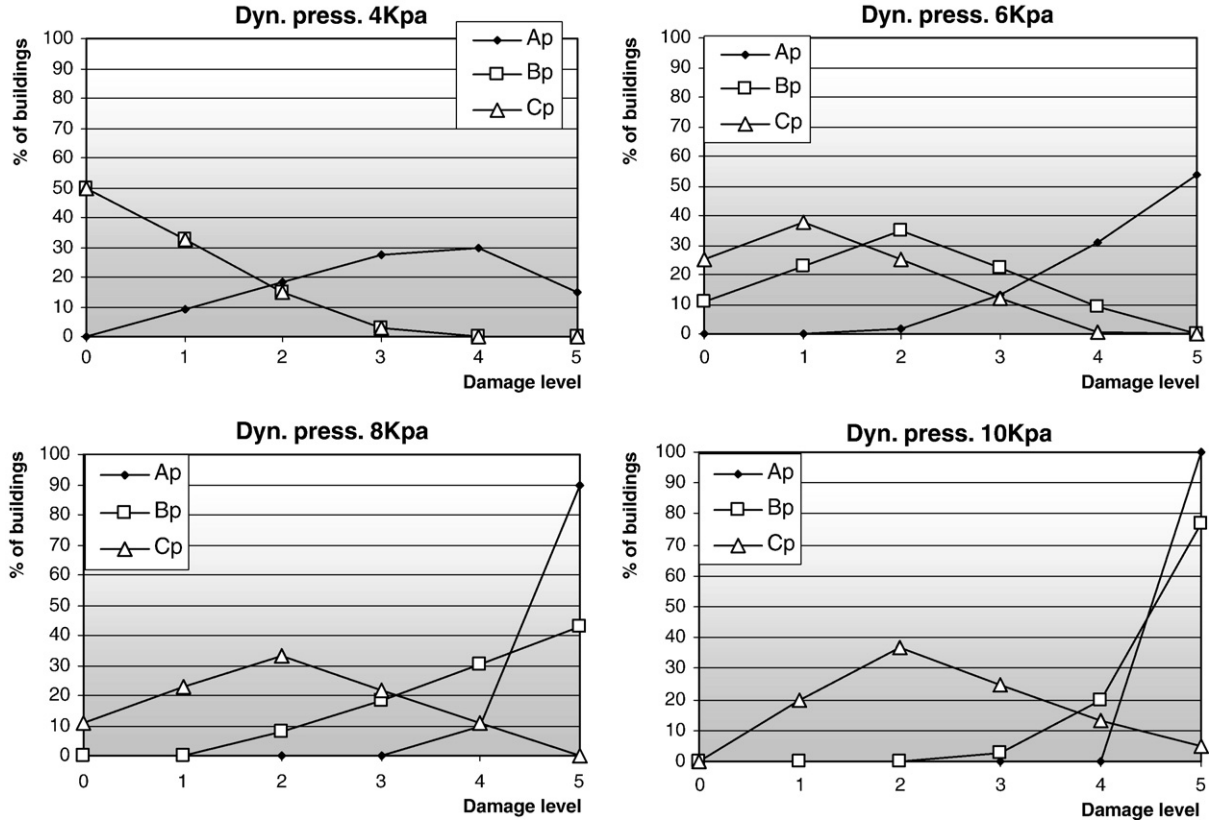

Fig. 8. Vulnerability functions for masonry building typologies A_p, B_p and C_p under the action of pyroclastic flow.

4.3.3. Reinforced concrete structures

Push over numerical simulations have been performed on real reinforced concrete buildings chosen as representative prototype of urban settlements in the Vesuvian area.

The evaluation of the limit horizontal pressures that the structures can resist has been performed by means of the fundamental theorems of the limit analysis, also factoring in the properties of the material (concrete and reinforcement), the particular feature of reinforced concrete structure of the area (local building rules) and the plan irregularities. Four different reinforced concrete structure typologies (strong aseismic, weak aseismic, strong non-aseismic, weak non-aseismic) have been considered (Fig. 9) (Zuccaro et al., 2000; Zuccaro and Petrazzuoli, 2004a). As a result, the limits of resistance for each typology, in the case of

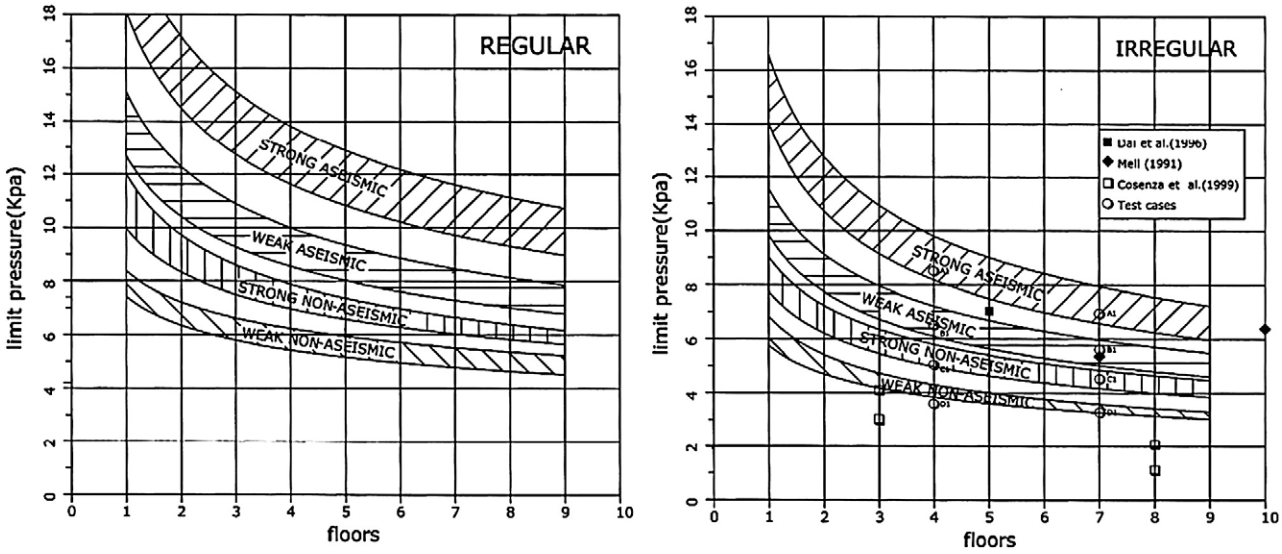

Fig. 9. Limit state functions of collapse for different reinforced concrete structural typologies under the action of a Low Density Current.

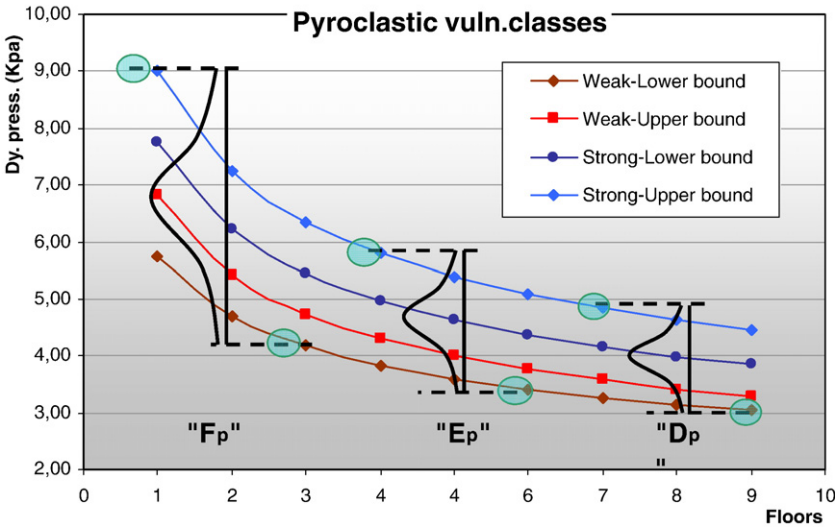

Fig. 10. Lower and upper bounds of the horizontal loads at the limit state of collapse derived for building types of different mechanical and geometrical characteristics. Identification of the vulnerability classes and their possible Gaussian probability distribution.

regular and irregular plan, are provided. Such limits of resistance are in good agreement with the literature data coming from the simulation of building collapses under seismic actions, since resistance to seismic actions is determined for a "push over" curve under horizontal load (Meli, 1991; Dai et al., 1996; Cosenza et al., 2000). The reinforced concrete structures show a large scattering of HPL (horizontal pressure limit) ranging from 3 to 5 kPa for tall weak and irregular non-aseismic buildings, up to values larger than 10 kPa for small strong aseismic buildings (see Zuccaro et al., 2000).

Considering that most people living in the area stay in reinforced concrete, buildings not designed to resist horizontal actions, the curves for only weak non-aseismic and strong non-aseismic buildings of irregular plan have been considered. Three different vulnerability classes have been then identified for R.C. buildings (D_p, E_p and F_p) according to the number of storeys. The lower and the upper bounds of the curves of Fig. 10 represent respectively the 5th and the 95th percentiles of the collapse probability obtained by Monte Carlo simulations at limit state of collapse on a simplified model. By means of standard deviation obtained from MC simulations a final set of vulnerability curves at the state of collapse having Gaussian Distribution has been derived for buildings with a given range of number of storeys.

Hence, the pressure causing damage class D5 (total collapse) has been derived. To produce a complete set of vulnerability curves for PF the resistance values of the structural and non-structural elements of the buildings (e.g. as windows, doors, and infill panels) tested in previous studies (Spence et al., 2004b) have been taken into account. A first attempt of a systematic evaluation of the reinforced concrete buildings resistance to a dilute horizontal current has been then computed. This result has to be considered as the first step toward a more confident assessment of such a kind of problem. Fig. 11 shows a sample of these vulnerability curves for building type D_p, E_p and F_p and for dynamic pressures 3 and 4 kPa derived from the binomial

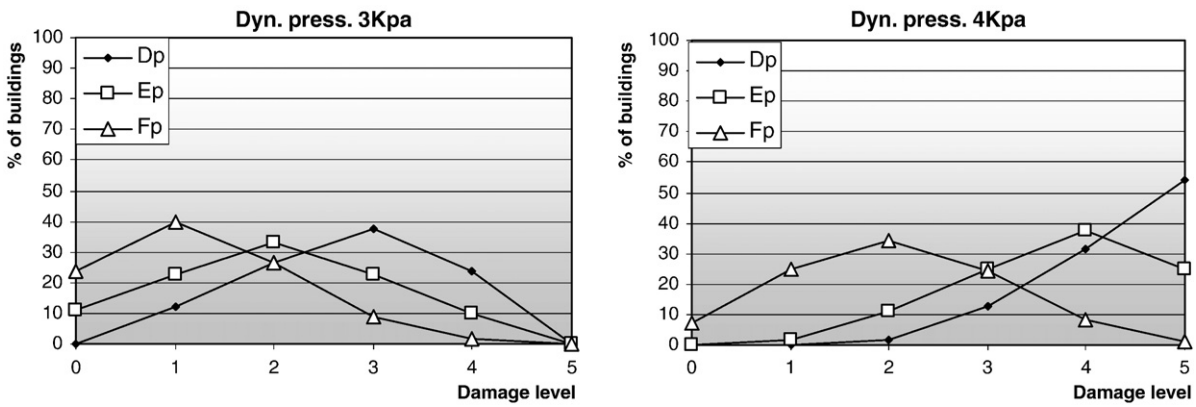

Fig. 11. Sample of vulnerability functions for reinforced concrete building types D_p, E_p and F_p.

Table 7
Percentage of window failure for different window class and dynamic pressure

Window class	Dynamic pressure (kPa)							
	0.5	1	1.5	2	3	4	5	6
Small	0	0	0	0	0.0002	0.038	0.354	0.7774
Typical	0	0	0.0007	0.0816	0.873	0.998	1	1
Large	0	0	0.0142	0.347	0.984	1	1	1

coefficients of Table 6(b) using the same technique described for the masonry buildings (see Zuccaro and Cacace, 2007a for details).

4.3.4. Non-structural element vulnerability (NSE)

The NSE vulnerability definition is crucial in the evaluation of structure and human damages due to PF actions. In the model, in spite of an extensive campaign of resistance tests performed on windows, doors, infill panels, partitions etc., only the effect on the structures and on the casualty due to windows failure has been considered. Future developments of the model will extend the influence of the other NSE (Baxter et al., 2004) on the final impact evaluation.

However all the information derived either from the numerical elaboration or from tests have been taken into account in the definition of the global state of damage of the buildings used to calibrate the PF vulnerability functions. Then the problem of windows failure is taken into account by the model separately by the impact damage evaluation on the structures.

The damage to the windows is caused either by dynamic pressure or the temperature of the flow.

The model allows the failure of windows to be evaluated by combining the data on the inventory of the windows classification for each building class (surveyed in the area) with tests and numerical elaborations on windows and shutters resistance (Spence et al., 2004b). Table 7 shows the values of the window vulnerability functions assumed in relation to window size.

For the other cause of window failure: the temperature tests performed in EXPLORIS have shown that non-protected windows fail at temperatures greater than 70 °C.

The failure of the windows determines the massive infiltration of hot ash (Spence et al., 2004a), moreover it has been evaluated that for temperatures greater than 250 °C fire breaks out in the buildings.

To determine the casualty consequent to the windows failure three possible cases have been considered:

1. *The pressure and the temperature are not enough to break the window, however infiltration of hot flow with toxic gas occurs.*
   In this case the casualties are evaluated on the basis of the seismic-building typology to which is assigned a capacity to resist to the infiltration; this is done using the casualty model by Spence et al. (2004a, 2007).
2. *The pressure and the temperature are enough to break the window, but the temperature is not high enough for the ignition of the building.*
   In this case it has been estimated, using documents from Montserrat, that the 15% of the building occupants is injured and another 15% dies, see Spence et al. (2007).
3. *The pressure and the temperature are such to break the windows and the temperature is high enough that in the building the fires break out.*
   In this case the model considers that the 45% of the building occupants is injured and another 45% dies.

Other factors influence the final casualty evaluation computed by the model when the windows don't fail, as the inside temperature of the buildings see Baxter (1990), Baxter et al. (1998) and Spence et al. (2004a) for more details.

5. Combined vulnerability

5.1. Ash fall followed by earthquake

As discussed above (see Section 2), up to now, two cases of coincident action have been examined. The case here presented is when an earthquake occurs after or during the ash fall deposit (AF → EQ). According to some historical documents on Vesuvius eruptions (Rosi, personal communication), the combination of ash fall and seismic action is one of the main possible reasons of collapse for masonry structures which survive (or which did not experience) pyroclastic flows.

In order to understand the influence of ash deposit on masonry and R.C. structures under seismic excitation, an iterative Limit State Model "SHREC" (Structural Horizontal Resistance Evaluation at Collapse), (Zuccaro et al., 2000; Zuccaro and Petrazzuoli, 2004a) has been applied to typical building typologies of Vesuvian villages by varying randomly the structural characteristics both in geometry and in mechanical parameters of the material. A simplified model under the combination of ash vertical loading and horizontal seismic action has been investigated. First, the collapse load multiplier under the vertical load has been studied. Second, the decay of this collapse multiplier under the horizontal seismic action has been evaluated. The response of the parameters describing the structural geometry and the seismic input are also considered (Zuccaro 2000; Baratta et al., 2004; Zuccaro and Petrazzuoli, 2004a).

An almost linear decrease of the seismic response with ash load has been observed (Fig. 12). In particular, consider a structure that reaches the collapse limit for a horizontal limit coefficient of C_o=0.1 (Baratta et al., 2004). If loaded by an ash

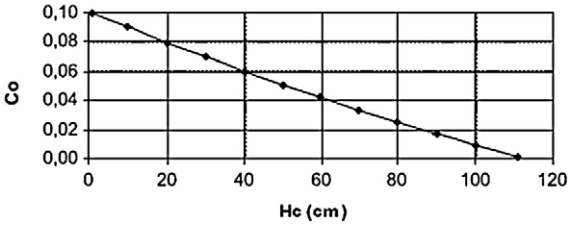

Fig. 12. Horizontal collapse multiplier (C_o) against ash deposit thickness (H_c) for masonry buildings.

Table 8
Seismic intensity increment for corresponding ash loads

Type	3	4	5	6	7	8	9	10	11	12	13	14	15	16	17	18	19	20
	(kPa)																	
A_s	$I+1$			$I+2$			$I+3$			$I+4$			$I+5$					
B_s		$I+1$				$I+2$				$I+3$				$I+4$				$I+5$
C_s			$I+1$					$I+2$					$I+3$					$I+4$
D_s				$I+1$						$I+2$						$I+3$		

deposit H_c of 60 cm which is taken for this calculation to be equal to 600 kg/m^2 load (assuming the density equal to 1000 kg/m^3), this structure reaches the collapse limit for a horizontal limit coefficient of $C_o=0.04$.

This result, valid both for masonry and for R.C. structures may be taken to correspond to an increment of felt macroseismic intensity because of the ash deposit on the roof, alternatively it could be interpreted as a decrement of vulnerability building class. In the case reported above it has been evaluated that 600 kg/m^2 of ash load determines a shift of two intensity classes.

Therefore a general law to increment the real seismic intensity in presence of ash load on the roof is proposed. In Table 8 the increments of the seismic action (expressed in equivalent intensity) for different vulnerability building classes corresponding to increments of ash load are reported.

Hence to evaluate the damage distribution in case of earthquake occurring after or during ash fallout the seismic DPM reported at Section 4.1 can be used, considering the intensity incremented as shown in Table 8 according to the ash load (Zuccaro, submitted for publication).

5.2. Ash fall followed by pyroclastic flow

The structural response under the load combination due to ash fall and pyroclastic flow has been evaluated taking advantage from the numerical models of masonry and R.C. structures discussed in Section 4.3. The study has shown the positive effect of the vertical ash load on the roof that, when it does not reach the value of the roof collapse, produces on the structure a considerable stabilizing effect due to the total weight increment.

The set of the numerical models studied have been subdivided according to the vertical ash fall load considered. Several classes of ash deposit have been considered with incremental steps of 30 cm.

The density assumed is 1000 kg/m^3, i.e. 1 kPa every 10 cm of ash deposit; Table 9 reports the results of the Monte Carlo simulation performed by using the SHREC Model for a sample of the ash load classes considered.

In order to facilitate the reader in the evaluation of the resistance increment, the dynamic pressure corresponding to limit state of collapse in the absence of ash fall deposit is also reported in the first columns of the table.

The parameter of the resistance increment (RI) shown in Table 9 $RI_{K,L,D5}$ (where K = typological class, L = ash fall load, D5 = damage level 5 "collapse") is derived as the ratio between the mean value of the dynamic pressure (DP) at limit of the collapse with and without the presence of the ash deposit on the roof.

The values in Table 9 are referred to DP of collapse (damage D5); it has to be underlined that the influence of the ash fall load on the damage of non-structural element due to PF is very low, therefore it has been neglected.

These resistance increment factors RI modify the PF–DPM relevant to the structure typologies by altering the correspondent binomial coefficients through the formula:

$$p_{K,Q} = p_{K,0} - p_{K,0} \cdot RI_{K,Q} \tag{3}$$

where

$p_{K,Q}$ is the binomial coefficient relevant to the PF vulnerability (structural typology) classes (K=A,B,…, F) and Q is the ash fall vertical load.

$p_{K,0}$ is the binomial coefficient relevant to the PF vulnerability (structural typology) classes (K=A,B,…, F) without considering the presence of the ash fall deposit.

$RI_{K,Q}$ the percentage of increment of structural resistance.

Table 9
Dynamic pressures (kPa) factor of resistance increment (RI) of structures under PF in presence of ash fall load on the roof

Ash deposit→	0			3				6				9			
	(kPa)														
Building class	Min	Max	Mean	Min	Max	Mean	RI%	Min	Max	Mean	RI%	Min	Max	Mean	RI%
A_p	1.40	4.99	3.195	1.60	5.60	3.6	12.68	2.70	6.20	4.45	39.28	1.80	6.70	4.25	33.02
B_p	3.89	17.70	10.795	5.50	18.40	11.95	10.70	6.98	22.30	14.64	35.62	8.30	25.80	17.05	57.94
C_p	8.40	19.10	13.75	11.26	24.20	17.73	28.95	13.90	29.70	21.8	58.55	17.10	33.50	25.3	84.00
D_p	3.04	4.85	3.945	3.00	4.95	3.975	0.76	2.99	5.01	4	1.39	2.98	5.05	4.015	1.77
E_p	3.42	5.80	4.61	3.50	6.11	4.805	4.23	3.58	6.40	4.99	8.24	3.61	6.55	5.08	10.20
F_p	4.18	9.02	6.6	4.56	10.26	7.41	12.27	4.87	11.72	8.295	25.68	5.02	12.46	8.74	32.42

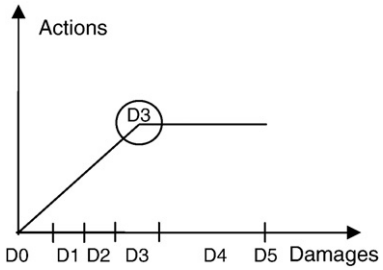

Fig. 13. The ideal elasto-plastic model and the critical damage D3 range.

The damages on the buildings affected by the PFs are then derived by taking the appropriate binomial coefficient according to the ash load on the roof and developing the DPMs by Eq. (2). When $p_{K,Q}>1$ the model considers the building has lost any resistance capacity therefore the binomial coefficient is assumed as the maximum possible (0.99).

6. A procedure for the cumulative damage evaluation during the eruption

The final impact scenario can be determined by a parametric analysis of the cumulative damage that the structure experiences in the possible sequence of events. The problem can be treated as a progressive deterioration of the building's resistance characteristics as represented by the damage level.

Assuming that the structures can survive numerous moderate events when the "elastic threshold" (conventional for masonry buildings) is not exceeded, and assuming that this corresponds to a damage level $\leq$ D3, we can calibrate a model of cumulative damage due to the sequence of events on the structures. An ideal elasto-plastic model is assumed with damage D3 range centred on the elastic limit (see Fig. 13).

The total damage suffered by the buildings during the whole eruptive process is evaluated using a computerised model prepared for the purpose. This allows to simulate the building damage distribution in the area caused by the sequence of seismic events, by the accumulation of vertical load due to ash fallout and by the lateral pressure consequent to the pyroclastic flows.

An important characteristic of the model is the capability to "recalibrate itself" during the event sequence, updating dynamically the building inventory and the vulnerability functions.

The sequence of the events simulated can be built either on the basis of the studies of past eruptions or on expert evaluations; for example the Sub-Plinian I-like eruption could be described by:

- a sequence of seismic events, during the unrest phase, with an increasing release of energy, up to the peak of seismic activity that is probably immediately before the explosion,
- a phase of ash fall, about 12–18 h long, during which there is a growing accumulation of ash (depth increasing linearly with time, Macedonio et al., 2008-this issue) on the roofs. During this phase it is possible that one or two seismic events occur with smaller intensity than the peak of the previous phase,
- a final phase, 2–5 h long, during which in several zones some buildings are affected by a lateral pressure and high temperature due to pyroclastic flows. In this phase a given number of pulses are considered.

The study area has been subdivided into cells using a circular grid centred on the crater (Fig. 14). By using an

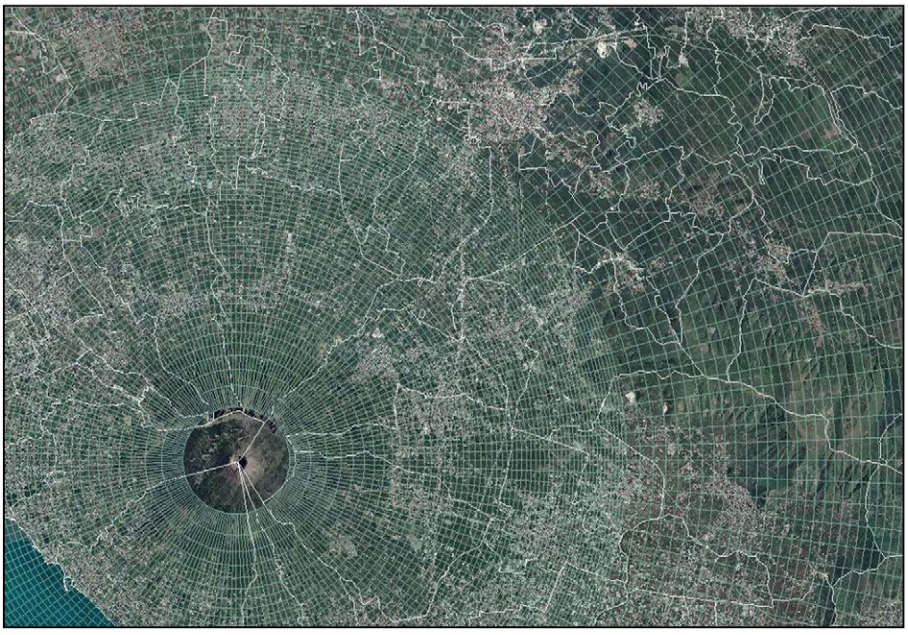

Fig. 14. Grid overlapped to the studied area.

Fig. 15. A detail of the grid with seismic class distribution of the buildings.

automatic GIS script the building inventory of the vulnerability classes in the single cell of the grid is updated by shifting the class according to the damage caused by the previous event and so on. When the cumulative damage to the building becomes equal to or bigger than damage state D4 the model considers it destroyed.

The choice to allocate the input data or the results to the cells of the grid follows three basic rules:

1. The information on the building type characteristic required to determine structure the vulnerability against the three possible phenomena considered (EQ, AF, PF) are not always available (more than 65% of the building heritage of the Vesuvian villages has been surveyed, however the 35% has still to be investigated). Moreover for the building in the Red Zone (the villages around the volcano) the seismic vulnerability classification (Ks) is only known, therefore the other vulnerability classifications (Kr and Kp) are statistically derived from the correlations between the vulnerability classes based on a robust sample. Hence the building class distribution is assessed according to the building population of the cell.
2. The building damage assessment consequent to a given level of external action (i.e. seismic excitation, ash load or pyroclastic flow) is probabilistically based. Therefore the expected distribution of damage is obtained as probabilistic

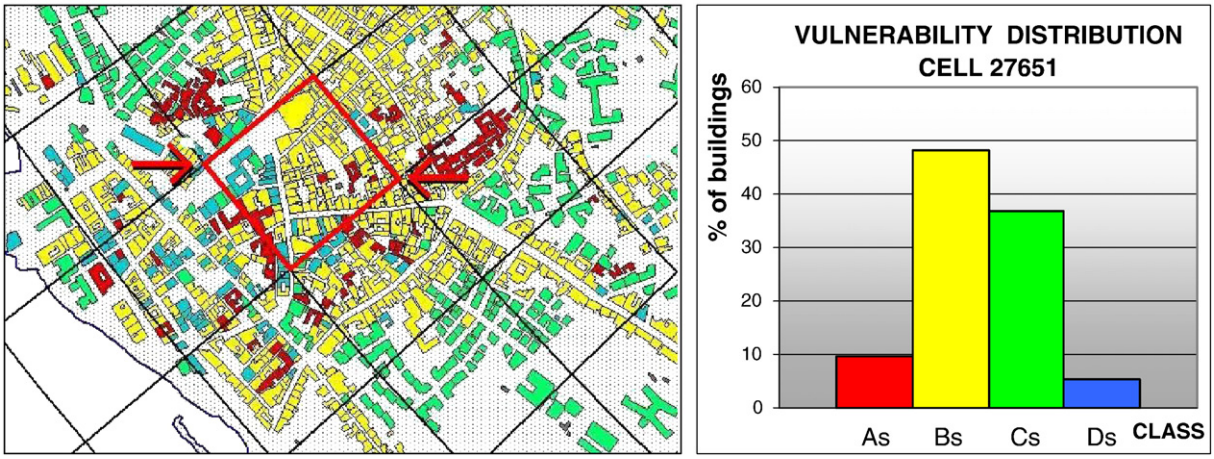

Fig. 16. Seismic class distribution for the cell no. 27651.

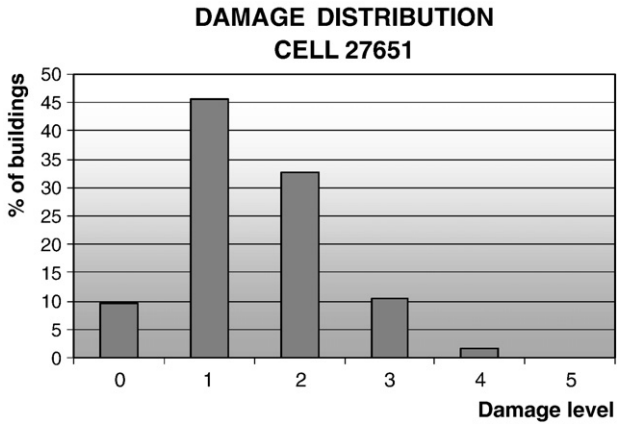

Fig. 17. Seismic damage distribution due to a local EQ intensity of VII felt in cell no. 27651.

distribution of the damage on the building population of the cell rather than for the single building of a given class.

3. The assumption of a spatial grid allows an effective geographic presentation of the data and of the results addressed especially from scenario elaborations.

In the following sections a hypothetical eruptive sequence is reported and the logic of the model described.

6.1. Earthquake sequence (Phase 1)

Consider that the inventory of the elements at risk in the study area have been subdivided in the cells of the grid and the distribution of the single seismic typological classes (A_s, B_s, C_s, D_s) is there assigned. The correlations between the seismic typologies and the typological classes of the other phenomena: AF and PF allow the complete building characteristic distributions to be assigned (Fig. 15).

In Fig. 16 a sample of the seismic vulnerability class distribution of the buildings for a particular cell is shown; on these buildings the action of the first seismic event of the sequence is considered, this determines a damage distribution (Fig. 17), according to the EMS scale, that can be evaluated using the vulnerability functions (DPM) above described.

The damage from this event modifies the capacity of the buildings to resist the following actions (EQs, AFs, PFs) therefore the inventory of the buildings population in the cell changes.

A routine has been developed to estimate the deterioration of the building resistance due to previous damage and to assign, proportionally to the level of the damage recorded after the event, a virtual vulnerability class that will address the choice of the DPM to be used for that building when the following event occurs.

In detail:

- If the building has not been damaged (D0) or has suffered only light damage (D1) that has not violated the integrity of the structural elements it preserves the vulnerability class it had before the event.
- If the building has suffered damages D2 (light structural damage), the vulnerability level will be increased of one class.
- If the building has suffered heavy damages (D3) the vulnerability degree will be increased of two classes.
- If the building has suffered damages D4 (partial collapse) or D5 (total collapse) it is considered "lost" and it goes out of the population of buildings of the cell in the elaborations of the damage for the following events.

In Fig. 18 the system to take into account the deterioration of the vulnerability classes is better clarified.

In Fig. 18 two new DPMs appear: DMP (A−) and DPM (A−−); these two new vulnerability functions take into account the resistance deterioration of the most vulnerable building class "A" when this does not collapse after a seismic event and to supply the DPM to be used for the following event.

These two DPMs have been derived by extrapolation of the binomial coefficient for the standard vulnerability classes (A_s, B_s, C_s, D_s) calibrated through the damage database of the previous seismic events in Italy (Zuccaro and Baratta, 1999; Zuccaro, 2004; Cherubini et al., 2002; Zuccaro and Cacace,

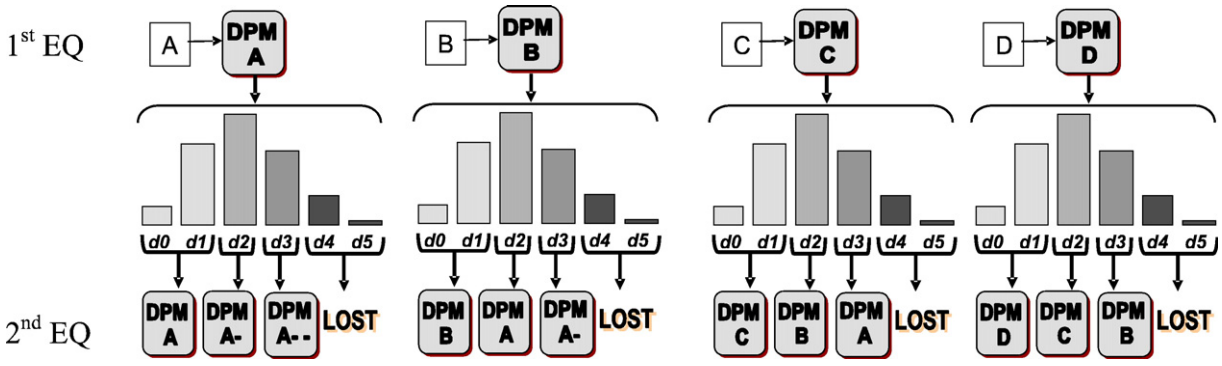

Fig. 18. The system to process the buildings affected by a seismic event sequence.

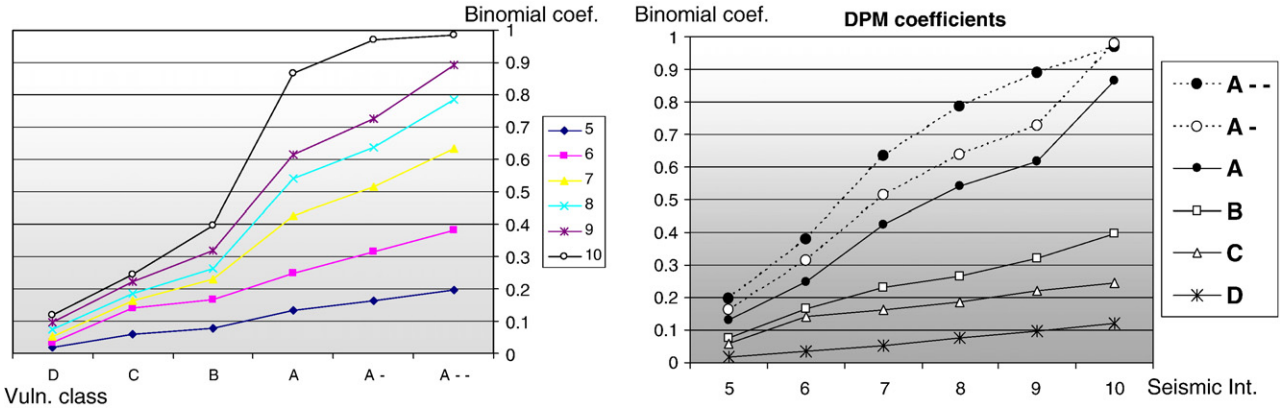

Fig. 19. The extrapolation of the binomial coefficients for virtual vulnerability classes "A−" and "A−−" (on the left) and the final DPM binomial coefficients adopted (on the right).

2007a) available at PLINIVS–LUPT Study Centre of the University of Naples.

In Fig. 19 the result of the "step interpolation" is reported; once the binomial coefficients are determined through Eq. (2) the DPMs "A−" and "A−−" can be computed. The model keeps the information of the original seismic typological class since this is important to the possible further evaluations of damage based on the specific characteristics of that original typology due to other phenomena.

Therefore the memory of the deterioration of a specific building affects only the choice of the DPM to be used for the following seismic event. This procedure is repeated for all the seismic events of damaging intensities considered in the seismic sequence during the unrest phase.

6.2. Ash fallout (Phase 2)

Once the eruption starts the ash fallout begins; during this phase the model considers a progressive increment (linear in time) of the ash deposit dispersion on the territory following a pre-determined ash fall footprint that is transformed into vertical load on the roofs either in the Red Zone or in the Yellow Zone. The ash fall footprint has been provided by Macedonio et al. (2008-this issue) on the basis of the average deposit dispersion in each of the eight (45°) radial sectors in which the territory potentially affected by the eruption has been subdivided.

The ash fall load distribution acts on the inventory updated to the last damage distribution due to the previous seismic sequence of the first phase, therefore the buildings damaged at D4 or D5 level are considered lost and eliminated from the inventory of the cell.

The roof resistance of the buildings is considered not influenced by previous seismic damages.

The model allows this phase to be divided into n time intervals, and it appraises the effects on the buildings in correspondence to the final instant T_{ni} of every interval.

The inventory is updated at every time step attributing the level of damage D4 (partial collapse) to the buildings for which the load overcomes the limit threshold of the corresponding vulnerability class. These are considered "lost" and eliminated by the population of buildings of the cell.

6.3. Seismic events during the phase of ash fall

Although the seismic activity reaches the maximum during the unrest phase, during the following ash fall phase some seismic events of minor intensity could occur.

In this case the building inventory altered by the damages due to the previous sequence of earthquakes plus the partial collapse of the roofs due to ash load is further modified by the damages consequent to the combinations of the seismic and ash load actions. The damage distribution is derived applying the right DPMs according to the virtual vulnerability class of the building at the end of the previous damaging sequence (see Section 5).

The procedure carries on the progressive increment of the ash load step by step and finally achieves the maximum at the end of the 2nd Phase; the damage distribution is evaluated as described in previous paragraphs.

6.4. Pyroclastic flows

The model simulates the pyroclastic flows action by generating a sequence of impulsive events; these are realized by loading the buildings located in some preferential sectors around the crater with lateral dynamic pressure.

The structural response to the PF action depends on the specific building class characteristics, therefore the damage distribution is derived by the PF–DPMs according to the vulnerability class and lateral pressure of the flow in the cell.

Two factors influence the building response under the PF action:

- the positive stabilizing effect due to the ash load on the roof;
- the reduction of the building resistance due to damage derived from previous events.

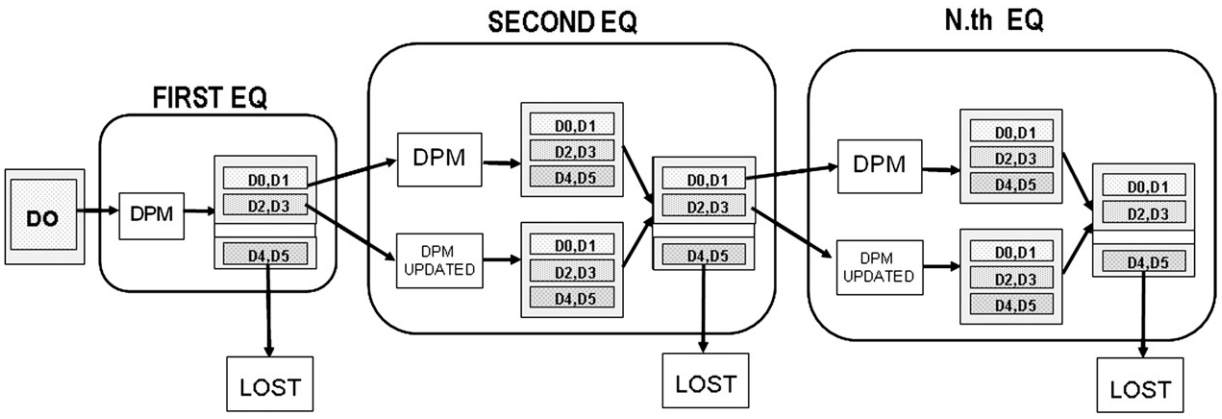

Fig. 20. The scheme shows the model logic tree for an Earthquake sequence.

The first factor has already been discussed above, the second is treated reducing the structure resistance proportionally to the damage registered on the structures itself after the previous events:

- the buildings experiencing damage levels D4 and D5 are considered "lost" and eliminated from the cell inventory,
- for the buildings with damages ≤ D3 the resistance reduction is introduced by applying a penalising factor β to the binomial coefficients of the PF–DPM. The calibration of β depends on many factors; it requires certainly further investigation; however it has been possible in first approximation to consider the factor β as proportional to the previous level of damage but independent of the original vulnerability class of the building.

We assume: $\beta_1 = 0.05$; $\beta_2 = 0.30$; $\beta_3 = 0.60$ respectively for the three damage levels D1, D2 and D3. Therefore the penalised binomial coefficients are:

$$P_{KJ}(D_L) = P_{KJ} + P_{KJ} \cdot \beta_L - P_{KJ} \cdot RI_{K,Q} \tag{4}$$

where:

- $P_{KJ}(D_L)$ represents the binomial coefficient of the building damaged:
  - K represents the typological class,
  - J is the dynamic pressure,
  - D_L is the damage of level L experimented by the building at the end of the previous sequence of events,
- P_{KJ} represents the binomial coefficient of the building non-damaged

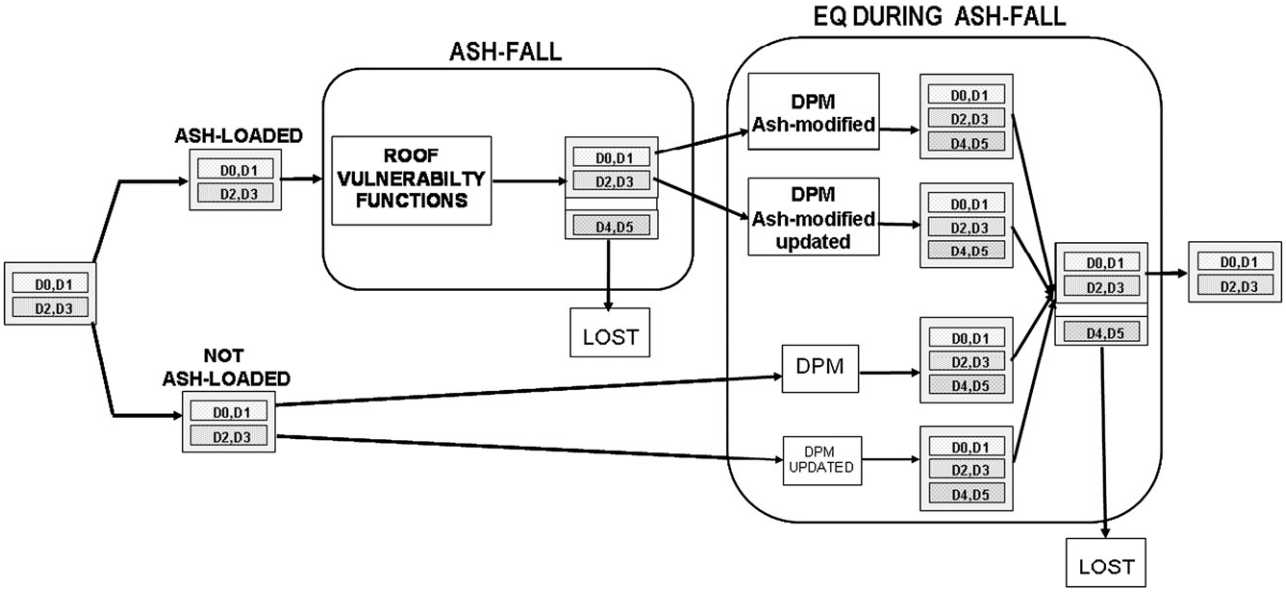

Fig. 21. The scheme shows the logic tree of the model for the ash fall phase including possible earthquakes occurring during this phase.

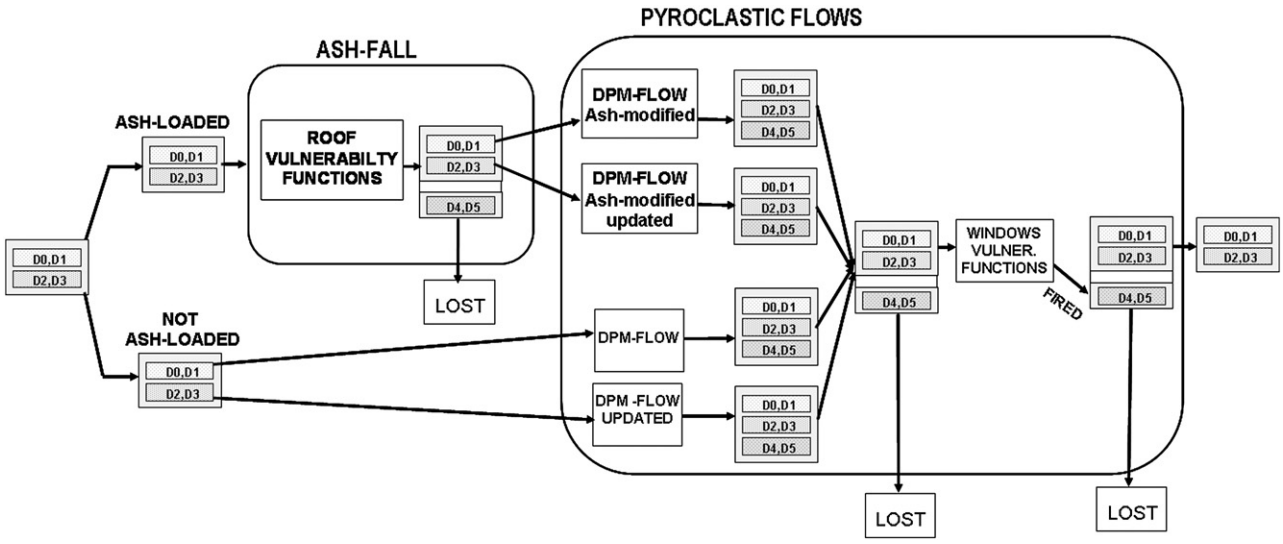

Fig. 22. The scheme shows the model logic tree for the pyroclastic flow phase including possible influence of the ash deposit on the roofs.

– β_L is the penalising factor from previous damage
– $RI_{K,Q}$ is the factor representing the improvement of the structural response because of the ash load Q.

The damage distribution due to PF is then derived from the DPM built up from the binomial coefficients modified $P_{KJ}(D_L)$.

As for the seismic sequence, the model evaluates the damages due to a given sequence of impulsive pyroclastic flows, the final damage distribution can be determined by iterating the procedure and updating at each step the binomial coefficients for each building types according to the damages recorded in the previous event.

6.5. The procedure run in synthesis — the single realization "Assigned Mode"

The dynamic process followed by the model is shown in a sequence of flow charts (Fig. 20).

The model keeps the memory of the cumulative damage registered on the buildings in the single cell of the grid after the seismic sequence.

Starting from the inventory damaged by the application of the seismic sequence, the model computes the further damage (D4 = partial collapse) due to the roof failures from ash fall (Fig. 21).

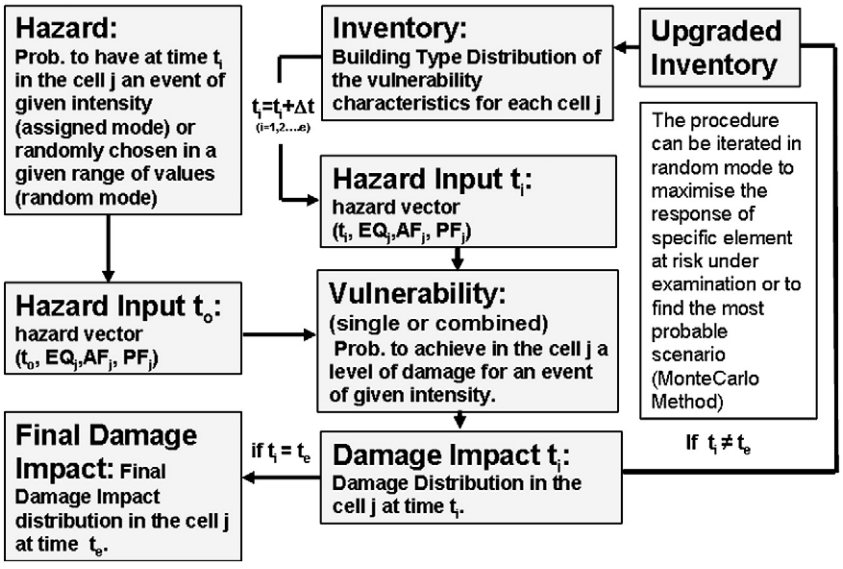

Fig. 23. The scheme of the "Random Mode".

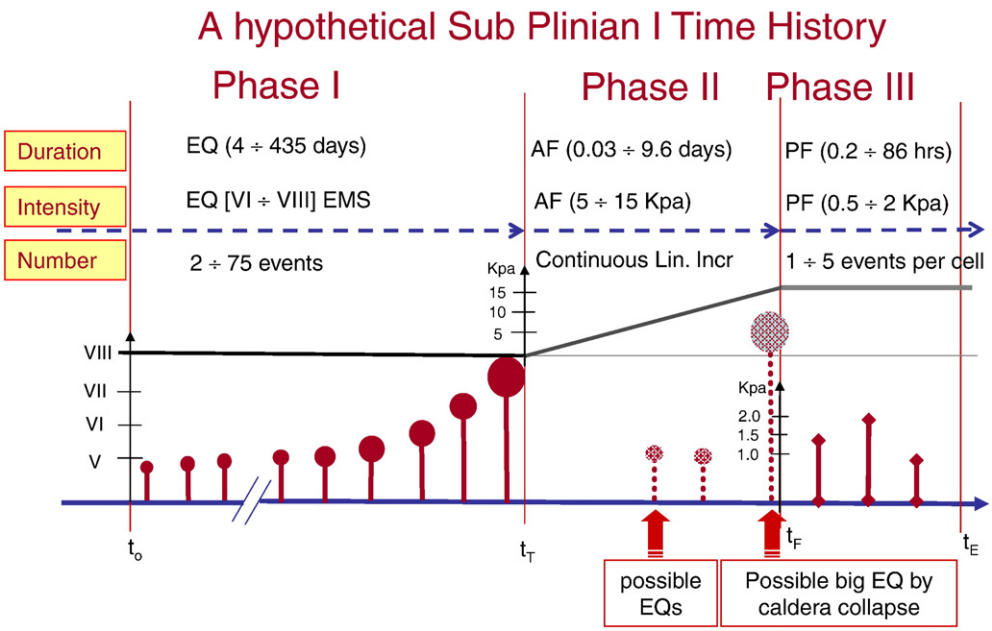

Fig. 24. Hypothetical Sub-Plinian I time history (the values and the symbols in the graph are hypothetical exemplifications; the diameter of the circle represents seismic intensity).

Then the model computes the cumulative damage on the buildings keeping the memory of the effects caused by the previous sequence of events (Fig. 22).

The schemes above describe one run of the model, it represents one realization of the uncertain variables to be evaluated obtained by a fixed input hazard vector (an application is shown in Section 8).

7. The model

7.1. The "Random Mode"

The goal of this model is the probabilistic evaluation of the damage impact scenario consequent to a given eruptive scenario (i.e. Sub-Plinian I-like) pursued through a routine able to simulate recursively *n* eruptive histories all compatible with the scenario assumed as input (Fig. 23).

In other words the "Assigned Mode" represents one single realization of the *n* recursive simulation performed in the "Random Mode". The following scheme describes conceptually the iterative mode (Zuccaro and Cacace, 2007b).

Table 10
Time-intervals elicitation

	Time	5%	50%	95%	Units
	Total duration of whole eruption	7.5	54	515	days
EQ	Med interval from Unrest to start A.F. (1st Phase)	4.3	46	435	days
AF	Med interval from start A.F. to start P.F (2nd Phase)	0.03	1	9.6	days
PF	Med duration of P.F. phase (3rd Phase)	0.2	5	86	hours

7.2. The parameters required

It is here reminded that for Sub-Plinian I eruption three phases can be identified:

- 1st Phase: (seismic phase) from the unrest instant t_o to the eruption start.
- 2nd Phase (ash fall phase) from the starting of the eruption to the column collapse and the beginning of the pyroclastic flow phase. Some earthquakes are expected during this phase.
- 3rd Phase (pyroclastic flow phase) from the beginning of the PF to the end of the eruption.

Therefore to simulate recursively the eruptive process chosen the following inputs are required:

- a time history of each hazard,
- a compatible spatial distribution of each hazard,

Table 11
Earthquake parameters elicitation

	5%	50%	95%	Units
Intensity				
Maximum magnitude of biggest seismic event	4.2	4.8	5.7	Magnitude
Average magnitude value for all seismic events with magnitude>3	3.3	3.7	4.3	Magnitude
Number of events				
Max number of seismic event per day with magnitude>3	2	25	75	Number
Average number of seismic event per day with magnitude>3	5	150	500	Number

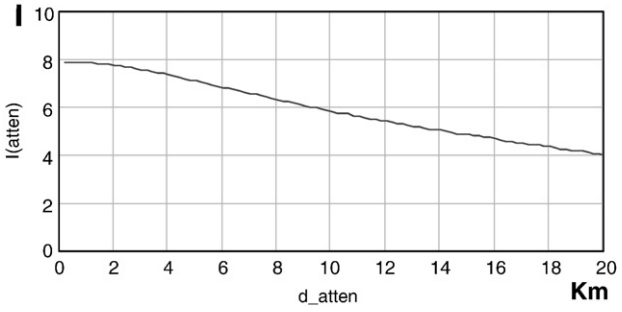

Fig. 25. Seismic attenuation law in the Vesuvian area (I = intensity, d = epicentral distance).

– compatible ranges of the values of the parameter describing the hazard input of each event (EQ, AF, PF) considered.

In order to parameterise the input of the impact model a possible set of input data can be listed:

EP1) the total duration of the eruptive process (EP), from the unrest instant t_o to the end of the eruption t_E
EQ1) the duration of the seismic phase from the unrest instant t_o to the explosion t_T (Phase 1);
EQ2) the number of precursors seismic events in $t_T - t_o$;
EQ3) the magnitude range of the earthquakes;
EQ4) the probable epicentral locations;
EQ5) the propagation of the seismic shaking through the region (attenuation law);
EQ6) the characteristics of one damaging possible seismic event of minor intensity during the AF phase, to be determined by definition of:
  a. the number of possible seismic events during Phase 2;
  b. the magnitude range of the earthquakes during Phase 2;

Table 12
Seismic intensity expected in the Vesuvian area

Intensity	5%	50%	95%	Units
Maximum intensity expected	VI	VII	VIII–IX	EMS
Average intensity	IV	V	VI–VII	EMS

EQ7) the eventuality (option ON/OFF) to include in the simulation a strong magnitude earthquake in case of caldera collapse approaching the end of the AF phase;
AF1) the duration of the ash fall phase, from the beginning of the explosion t_T to the collapse of the column and the beginning of the pyroclastic flows t_P (Phase 2);
AF2) the spatial distribution in the region of the ash deposits, determined by assigning the azimuthal direction of the wind (Macedonio et al., 2005; Costa et al., 2006). The consequent load distribution parameters are derived by numerical simulation model of the ash dispersion.
PF1) the duration of the pyroclastic flow phase from the beginning of the pyroclastic flows t_P to the end of the eruption t_E (Phase 3);
PF2) percentage of the mass collapsed and transformed in PFs;
PF3) number of the pulses for each alignment from the crater to the runout distance;
PF4) dynamic pressures along the alignments considered;
PF5) temperature along the alignments considered;
PF6) the spatial distribution in the region: azimuth direction for each PF;
PF7) the spatial distribution in the region: width of the damaging front as a function of the distance from the vent.

7.3. A sample of input variables calibration

In this section a possible process to calibrate the input variables of the model is shown.

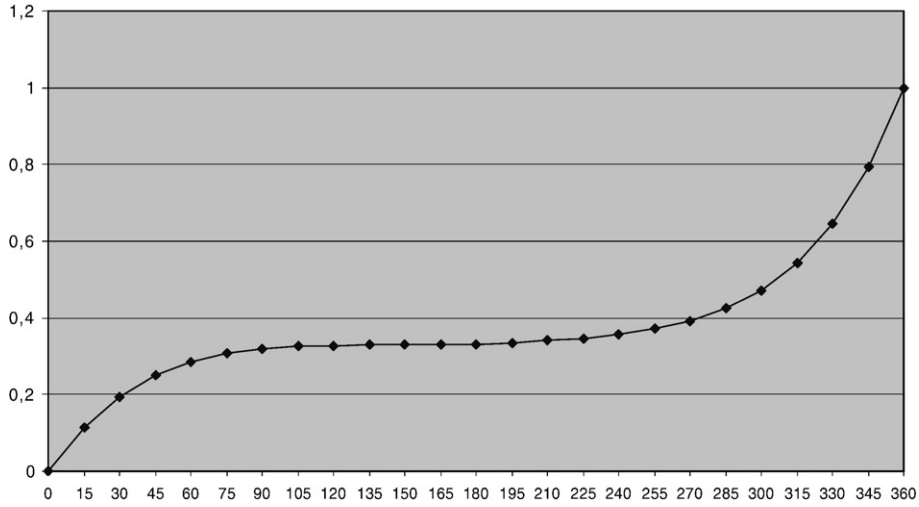

Fig. 26. Cumulative probability function of the wind direction at Mont Vesuvius. On the abscissa the angles of the principal axis of the elliptical ash dispersion with respect to EST direction clockwise (statistic elaboration from NOAA date, Kalnay et al., 1996).

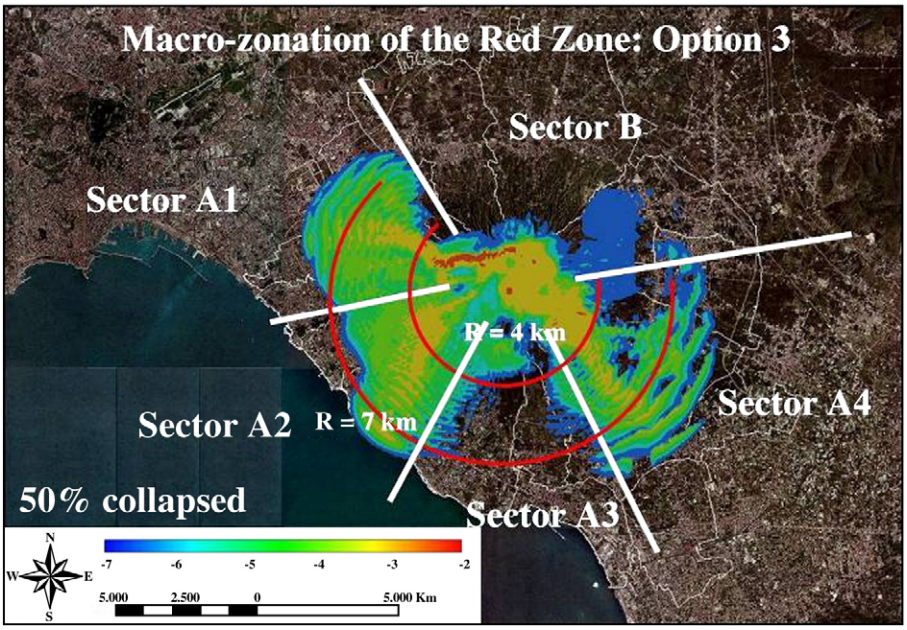

Fig. 27. Sectors considered for the elicitation on the pyroclastic flow distribution at Vesuvius (the scale represents the $\log_{10}$ of the total concentration of the particles after 1500 s, assuming the 50% of the mass collapsed, Neri et al., 2008-this issue).

7.3.1. Eruptive process (EP)

An example of hypothetical eruptive time history of the phenomena is reported in Fig. 24 for a Sub-Plinian I-like event.

For each of these parameters the probable range of variation is defined using:

- Chronicles of past events
- Numerical simulation models
- Elicitation techniques.

The time-progress of the eruption (parameters EP1, EQ1, AF1, PF1) can be evaluated using the probabilities of non-exceeding elicitated among a group of experts and reported in Table 10 (Aspinall, 2006; Aspinall et al., 2008-this issue).

Table 13
Probability of PF invasion for the sectors in Fig. 27

Space	5%	50%	95%	Units
PF invade Sector A1?	67	95	99.95	Prob (%)
PF invade Sector A2?	67	94	99.95	Prob (%)
PF invade Sector A3?	50	92	99.90	Prob (%)
PF invade Sector A4?	67	94	99.90	Prob (%)
PF invade Sector B?	10	45	84.00	Prob (%)

Table 14
Probability of PF max runout distance in the sectors of Fig. 27

Space	5%	50%	95%	Units
Maximum runout distance of PF into Sector A1?	2.5	7.6	13.3	km
Max runout distance of PF into Sector A2?	2.5	7.8	13.3	km
Max runout distance of PF into Sector A3?	2.3	7.5	13.2	km
Max runout distance of PF into Sector A4?	2.3	7.6	13.3	km
Max runout distance of PF into Sector B?	1.2	5.4	11.9	km

7.3.2. Earthquakes (EQ)

The number of seismic events and the maximum magnitude (EQ2, EQ3) can be evaluated by the critical analysis of the chronicles of past eruptions. In other way a probabilistic model based on the elicitated probabilities shown in Table 11 can be developed using the Gutenberg and Richter law (Gutenberg and Richter, 1956) to determine the magnitude distribution.

The determination of the epicentral locations requires the definition of the potential seismogenetic areas. These have been

Table 15
Probability of non-exceeding PF — peak dynamic pressure (PDP) and peak temperature (PT) in the sectors of Fig. 27 at 4 km (a) and 7 km (b) from the vent

Intensity	5%		50%		95%		Units	
a)								
PDP and peak temperature at 4 km into Sector A1	1.8	136	7.1	440	18.7	775	kPa	°C
PDP and peak temperature at 4 km into Sector A2?	1.8	136	7.1	440	18.7	775	kPa	°C
PDP and peak temperature at 4 km into Sector A3?	1.7	136	7.0	440	18.7	775	kPa	°C
PDP and peak temperature at 4 km into Sector A4?	1.8	136	7.1	440	18.7	775	kPa	°C
b)								
PDP and peak temperature at 7 km into Sector A1	0.3	68	2.3	270	9.5	535	kPa	°C
PDP and peak temperature at 7 km into Sector A2?	0.3	68	2.5	270	9.5	535	kPa	°C
PDP and peak temperature at 7 km into Sector A3?	0.3	68	2.5	270	9.5	535	kPa	°C
PDP and peak temperature at 7 km into Sector A4?	0.3	68	2.3	270	9.5	535	kPa	°C
PDP and peak temperature at 7 km into Sector B?	0.1	44	1.5	222	8.8	520	kPa	°C

assumed corresponding to the vent area (EQ4), but the model also allows other possible areas to be chosen.

The law that describes the propagation of the seismic shaking from the epicentre (EQ5), once the magnitude of the event is fixed, has been inferred by the contribution paper by Del Pezzo and Zollo (2005), (Fig. 25).

The parameter chosen to measure the seismic shaking is the EMS '98 intensity; the transformation of the magnitude into epicentral intensity has been computed by the formula (Del Pezzo and Zollo, 2005):

$$I_0 = \frac{1.82 - M_s}{0.32} \tag{5}$$

where I_0 is the EMS epicentral intensity and M_s is the weave magnitude.

Hence it is possible to obtain the intensity values, see Table 12.

In Fig. 25 the attenuation law adopted (EQ6) is shown.

The maximum magnitude value expected by the elicitation (Table 11), that has a very low probability to be exceeded (5% prob. to exc. M=5.7), is very close to the maximum magnitude value expected by the experts (Del Pezzo and Zollo, 2005) that is M=5.5.

Obviously, as already remarked, the seismic input to the model can also be deterministic; by assigning a sequence of seismic events (with time, space and intensities given) according to historical reconstruction of past eruptions. This has been done in the application reported at Section 8.

7.3.3. Ash fall (AF)

The spatial distribution of the ash fall deposits has been evaluated by numerical simulation of the ash dispersal in the proximal and distal areas performed respectively by INGV Department of Pisa and of Naples.

The distribution of the ash deposit is derived in a deterministic way by mean of mathematical models of the plume dispersion HAZMAP (Macedonio et al., 2005; Costa et al., 2006) for distal areas and VOL–CALPUFF (Neri et al., 2003; Barsotti and Neri, in press; Barsotti et al., in press for proximal areas); the distribution is strongly governed by the direction of the wind; this is taken into account through a probabilistic approach. The probability of the wind direction is derived from the statistics of the NOAA (Kalnay et al., 1996) database containing the last 10 years of wind observations.

In Fig. 26 the probability density function of the principal wind direction is shown.

7.3.4. Pyroclastic flow (PF)

The parameters required for modelling the pyroclastic flow behaviour has been evaluated taking advantage of a set of numerical simulation of the pyroclastic flow propagation in the area developed within EXPLORIS Project by the INGV Pisa Department (Neri et al., 2008-this issue).

The observations of these simulations has enabled a study of the number and the direction of the pulses, the possible values of the dynamic pressure and temperature at first impact of the flow with urbanised barriers and the decay of these with the distance from the eruptive source.

This experience and the chronicles of past events have supplied the background knowledge to the volcanologist to assign a probabilistic evaluation to the parameters that govern this phenomenon. The area surrounding the volcano has been subdivided in four sectors: A1, A2, A3 and A4 where numerical simulation and chronicles had shown characteristics not too much dissimilar and B having characteristics substantially different from the other three sectors (see Fig. 27).

The probabilistic parameters for sector occurrence, temperature and dynamic pressure have been evaluated for each of these sectors through elicitations (Aspinall, 2006).

In the following questions and results of PF elicitation are reported:

1. Given 100 PDC-generating episodes at Vesuvius occurring during Sub-Plinian I events, what is the range of probabilities for PF invading each sector (Table 13)?
2. Given 100 PF-generating episodes at Vesuvius occurring during Sub-Plinian I events, what will be the range of maximum runout distance in each sector (Table 14)?
3. Given 100 PF-generating episodes at Vesuvius occurring during Sub-Plinian I events, what will be the range of peak dynamic pressure and peak temperature in each sector (Table 15)?

7.4. The probabilistic process

Assuming the percentiles (5%, 50%, 95%) of the parameters listed above were available either applying the statistical method shown above (elicitations) or any other equivalent techniques, it can be assumed that the cumulative distribution of probability density function (PDF) for each parameter can be represented by a Beta distribution.

$$f(x;\alpha,\beta) = \frac{1}{B(\alpha,\beta)} x^{\alpha-1}(1-x)^{\beta-1} \tag{6}$$

The interpolating function is defined for $0<x<1$; the coefficients α and β are estimated interpolating the function on the correspondent values of the known percentiles and where

$$B(\alpha,\beta) = \int_0^1 x^{\alpha-1}\cdot(1-x)^{\beta-1}dx \tag{7}$$

is the function that allow to normalise the values of $f(x)$ in the interval (0,1).

The moments of the Beta distribution are:

$$E(X) = \alpha/(\alpha+\beta) \tag{8}$$

$$\mathrm{Var}(X) = \alpha\beta/\left[(\alpha+\beta)^2(\alpha+\beta+1)\right]. \tag{9}$$

In the following the basic steps of the ith iteration of the recursive procedure is synthesised.

1) The value of $x_{1,i}$ is extracted in the interval (0,1) through a generator of random values having uniform probability distribution.

2) The total duration of the eruptive process (EP1) is then determined as a realization of the PDF $f_{EP1}(x_{1,i})$ of the parameter EP1 correspondent to the random variable $x_{1,i}$ extracted.
3) Similarly, the duration of the unrest (EQ1) that corresponds to the seismic pre-eruptive phase (Phase 1) is derived by the correspondent realization obtained by the PDF $f_{EQ1}(x_{1,i})$ of the parameter EQ1.
4) Again using the same random extraction $x_{1,i}$ the total number (N_3) of the precursor seismic events with significant magnitude ($M>3$) can be fixed by means of the PDF of the parameter EQ2: $f_{EQ2}(x_{1,i})$.
5) Another random[2] value $x_{2,i}$ is extracted to evaluate through the PDF of EQ3: $f_{EQ3}(x_{2,i})$ the maximum seismic magnitude expected M_{max}; the minimum magnitude is fixed in default ($M=3$) considering it the minimum magnitude value causing damages.
6) The magnitude distribution in the area is then estimated by mean of the Gutenberg and Richter relation (Gutenberg and Richter, 1956).

$$a - Mb = \mathrm{Log}\,(N_M) \tag{10}$$

where M is the magnitude and N_M is the number of events having magnitude $\geq M$; the values of the coefficients a and b can be determined assuming a known pair of values:
   – for $M=3$ the number of events is $N_M=N_3$
   – for $M=M_{max}$ one event is considered, hence $N_M=1$
7) N_3 seismic events are then generated; each of these have:
   – Epicentres located in the crater (the most probable option)
   – The magnitude of the events always greater than 3 (this is set by a separate random generator and taking advantage by Eq. (10))
   – The attenuation computed trough the law of Fig. 25 (Del Pezzo et al., 2005).
8) The 3rd random value $x_{3,i}$ is extracted to fix the total duration of the ash fall phase (Phase 2). This is obtained by the PDF of the parameter AF1: $f_{AF1}(x_{3,i})$.
9) The ash fall distribution on the territory has roughly an elliptic shape, the load density gets smaller with distance from the crater. Therefore the parameters concurring to describe the hazard input in this phase are:
   – The dimension of the principal axes of the ellipse
   – The maximum load density (in the proximal area)
   – The decay factor of the load density with the distance
   – The direction of the principal axes of the ellipse (principal direction of fallout).

   The first three parameters are assumed in default by the model on the basis of the numerical simulations preformed from INGV–OV (Macedonio et al., 2005; 2008-this issue; Neri et al., 2008-this issue) for the Sub-Plinian I-like eruptions performed for all the wind directions.

   The principal direction (azimuth) of the fallout (AF2) chosen in the ith iteration of the model is obtained by extraction of another random value $x_{4,i}$ at uniform distribution and substituting it in the wind direction PDF, $f_{AF2}(x_{4,i})$, of Fig. 26.
10) By extracting the 5th random value at uniform probability $x_{5,i}$ and substituting it in an ON/OFF probability function, the possibility of an earthquake of significant magnitude during the AF phase is determined (EQ6).
11) The relevant magnitude of this event is determined by separate random extraction using the Gutenberg–Richter distribution described above for the (N_3+1)th event with an upper bound limitation that exclude the M_{max} event. All the other parameters: epicentre location, attenuation law etc. are assumed as described above.
12) By extracting the 6th random value at uniform probability $x_{6,i}$ and substituting it in an ON/OFF probability function, the possibility of a strong earthquake due to a caldera collapse could be taken into account (EQ7). However in the EXPLORIS Project this possibility has not been elicitated so the PDFs relevant to the occurrence of the event and its magnitude evaluation are not available; therefore this feature of the model is not active.
13) The duration of the PF phase is estimated by extraction of a further random value $x_{7,i}$ and substituting it in the PDF of the parameter PF1: $f_{PF1}(x_{7,i})$.
14) Analogous to the AF phenomenon the evaluation of the parameters to estimate the impact on the territory around the Vesuvius consequent to the PFs action has been assessed either by taking advantage of the numerical 3D simulations of the INGV Pisa (Neri et al. 2008-this issue) or by the elicitation results. In detail the parameters describing the hazard input of this phase are:
   – % of mass collapsed (PF2)
   – statistics of the number of the pulses (PF3)
   – statistics of the dynamic pressure (PF4)
   – statistics of the temperature (PF5)
   – spatial distribution in the region (PF6–PF7).

In spite of a complete set of elicitations available for all these parameters developed in the EXPLORIS Project, we have decided to assume only some of the PDFs derived from expert judgments and to complete the statistics using the INGV Pisa simulations. This choice that can be changed in any future simulation is justified by the consideration that some PDFs derived from the elicitations available seem to be too conservative compared with the numerical simulations. This suggested that, at this stage of the research, the statistics derived from simulations as input values should be taken as default values since it allows the efficiency of the model to be tested.

The statistics of the parameters from PF3 to PF5 for each sector (A1, A2, A3, A4 and B) of Fig. 27 are then obtained by the 3D numerical simulations files (Neri et al., 2008-this issue).

[2] The number of the events and the maximum value of the magnitude are here considered independent aleatory variables. This assumption could also be considered not correct if both depend by the value of the energy released before the eruption. However at the moment data to find this kind of correlation aren't available.

Therefore for each percentage of the mass collapsed assumed by the simulations of the INGV Pisa model (50%, 90%) mean and variance of the

- number of pulses (PF3) along the single PF alignment
- dynamic pressure at each cell of the alignment nearest the vent (PF4)
- temperature at each cell of the alignment nearest the vent (PF5)

for each sector are computed.

From the statistics of each parameters the PDFs are calibrated and by extraction of the random variable $x_{8,i}$ uniformly distributed the ith realization of PF3, PF4, PF5 computed.

The percentage of the mass collapsed could be set by extraction of a further random value at uniform distribution; however since the PDF of the percentage of the mass collapsed in PF is not available either by the results of the expert elicitations in EXPLORIS or from any other source it has been chosen to assume the most conservative option: 90% of the mass collapsed.

The spatial distribution is assigned by extracting other two random variables $x_{9,i}$, $x_{10,i}$. The first assigns the azimuth direction according to the PDF derived from the experts' elicitation on the invasion probability of the sectors (A1, A2, A3, A4 and B), while the second assigns randomly the width of the impact front of the single PF pulse in the range between 0 °C and the maximum angle fixed by the experts for the single sector.

A possible alternative in the definition of the parameters of this section of the model could consist of the definition of stochastic decay laws along each alignment for pressures and temperatures when more realizations of the 3D numerical simulations will be available and the PDF of the maximum values of dynamic pressure DP_{max} and temperature T_{max} in the areas proximal to the crater either from 3D simulations or from the experts' elicitation will be more consistent with each other.

A further decay factor due to the effect of urbanisation density on the flow pattern has been studied in EXPLORIS (Zuccaro and Ianniello, 2004b) but not included at the moment in the model; further developments of the research will include it.

The duration either of the total eruption or of the single phases doesn't influence the impact results evaluated by the model; however it has been included either for completeness of the time history definition or for Civil Protection applications.

Summarising, in addition to the random tool generator that feeds the Gutenberg–Richter seismicity law, the present version of the impact model requires 10 random extractions[3] to complete one iteration. Table 16 reports a synthetic scheme which shows both the input variables derived by extraction of random values (at uniform distribution) and relevant PDFs available or and those which are derived by a theoretical model that evaluates the single input through numerical simulations.

Table 16
Input variables: random and derived by theoretical models

Time history	Time distribution	Space distribution	Intensity distribution
Total eruption	EP1($x_{1,i}$)		
1st Phase	EQ1($x_{1,i}$)	Theoretical model	EQ2($x_{1,i}$)
			EQ3($x_{2,i}$)
			Theoretical model (T.M.)
2nd Phase	AF1($x_{3,i}$)	AF2($x_{4,i}$)	Theoretical model
			EQ6($x_{5,i}$)
			EQ7($x_{6,i}$)
3rd Phase	PF1($x_{7,i}$)	PF6($x_{9,i}$)	PF2 (90% mass collapsed)
		PF7($x_{10,i}$)	PF3($x_{8,i}$) statistics by T.M.
			PF4($x_{8,i}$) statistics by T.M.
			PF5($x_{8,i}$) statistics by T.M.

By a standard Monte Carlo simulation the most probable scenario is found and mean and variance of each parameter considered in the output results evaluated; the output of the model are:

- mean and variance of the number of buildings "lost" (D4+D5)
- mean and variance of the roofs collapsed
- mean and variance of the number of buildings ignited
- mean and variance of the windows failed
- mean and variance of the homeless (50% of D3+D4+D5)
- mean and variance of the number of victims (fixed the decay law for inhabitants in the area)
- mean and variance of the number of injuries (fixed the decay law for inhabitants in the area).

The procedure, as already mentioned above, allows also to estimate the maximum possible value of one specific output variable that can be found by maximising it along the iterations through a standard random walk optimization procedure.

8. Impact scenarios — *Sub-Plinian I*

The model, as described above, can either be used to find a single impact damage realization following a pre-determined time history of the eruption or to evaluate, enhancing the probabilistic approach, the most probable impact scenarios, building up numerous time histories using the procedure described in the previous paragraph. In this mode, by iterating the procedure in the "Random Mode", the model can also define the mode value of a single variable (i.e. number of buildings collapsed, number of roofs failed, number of homeless, etc.) varying randomly the input values in the credible ranges assessed by the experts.

The procedure presented has to be considered a tool to study possible impact scenarios of a given type of eruptive scenario and it has shown that to assemble all the knowledge required to achieve this result is possible.

[3] The random variable for the assignment of the % of mass collapsed is not considered since the relevant PDF is not available at the moment.

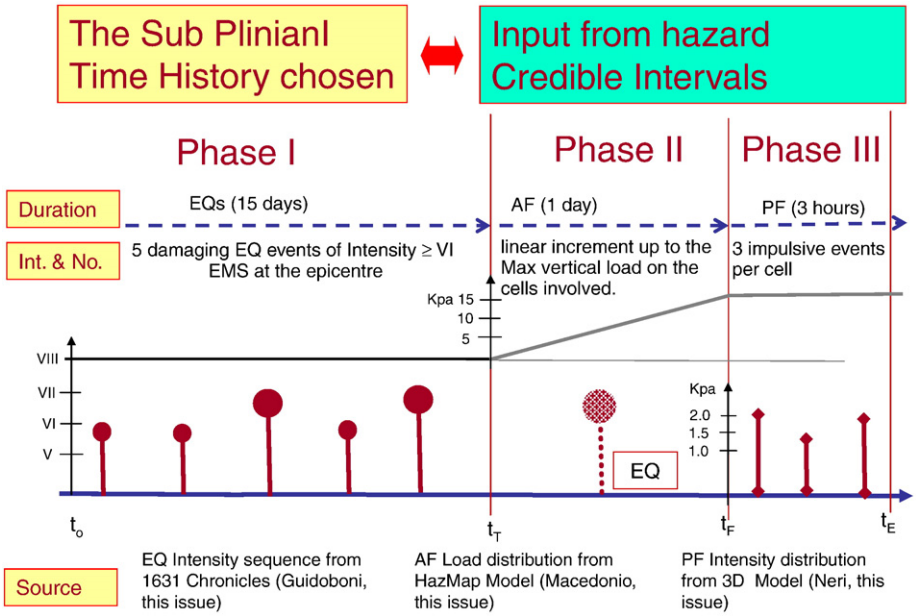

Fig. 28. The Sub-Plinian eruption time history chosen.

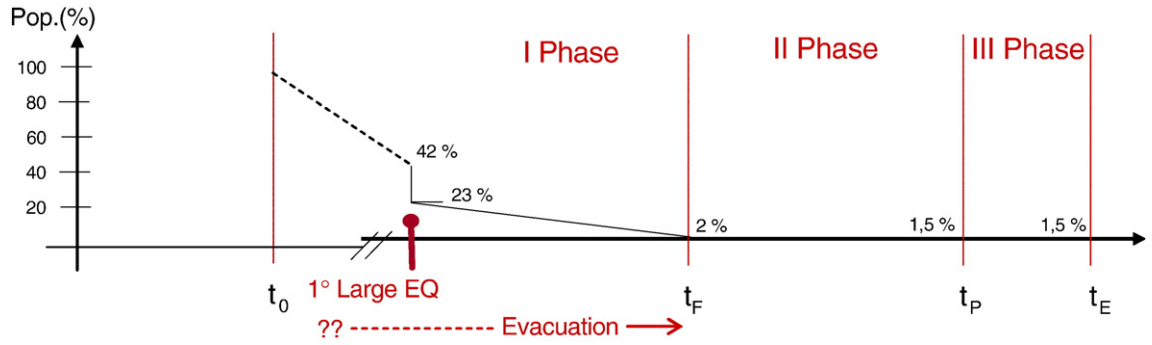

Fig. 29. Red Zone population decay law.

In this paragraph, a possible single realization of the impact damage scenario at Vesuvius in the Red and Yellow Zones of the CP Plan for a hypothetical Sub-Plinian I-like event, with characteristics as shown in Fig. 28, will be presented.

The model has an integrated software routine to evaluate the dynamical increment of possible casualties developed in collaboration with Cambridge University (see Spence et al., 2005). The Emergency Plan of the Italian Civil Protection foresees the complete evacuation of the population from the Red Zone before the eruption, however the model allows study of the possible evolution of the casualties once a decay law for inhabitants in the area is assumed and overlapped to the time history of the eruption. In order to test the feasibility of this kind of prevision and the possible implication in the emergency strategy, the exercise of considering some people remaining in the area during the eruption has been done. In Fig. 29 the hypothesis assumed regarding the population decay law in the Red Zone is shown.

8.1. Hazard input

8.1.1. 1st Phase

In this phase a sequence of 6 seismic events has been assumed following a sample of the seismic time history derived from chronicles (Carafa, 1632; Mascolo, 1634; Varrone, 1634) of the

Table 17
The damaging seismic events sequence of the 1631 eruption interpreted by (Guidoboni, 2008-this issue)

Year month day	Time	Site	Latitude	Longitude	Intensity
1631 12 16	4.00.00	Napoli	40,534,615	14,112,573	V–VI
1631 12 16	7.00.00	Napoli	40,450,322	14,274,354	VI
1631 12 17	9.00.00	Torre Annunziata	40,450,322	14,274,354	VII
1630 12 17	10.30.00	Area Vesuviana			V–VI
1630 12 17	11.00.00	Napoli	40,534,615	14,112,573	V–VI
1631 12 18	5.00.00	Torre Annunziata	40,450,322	14,274,354	VII

1631 eruption (the last Sub-Plinian I type eruption at Vesuvius). In Table 17 the values estimated are reported (Guidoboni, 2008-this issue). The last event occurs during the AF phase.

The model allows the damage to be followed dynamically *t*, growing step by step, this aspect produces results of great importance for the Civil Protection Authorities during the unrest

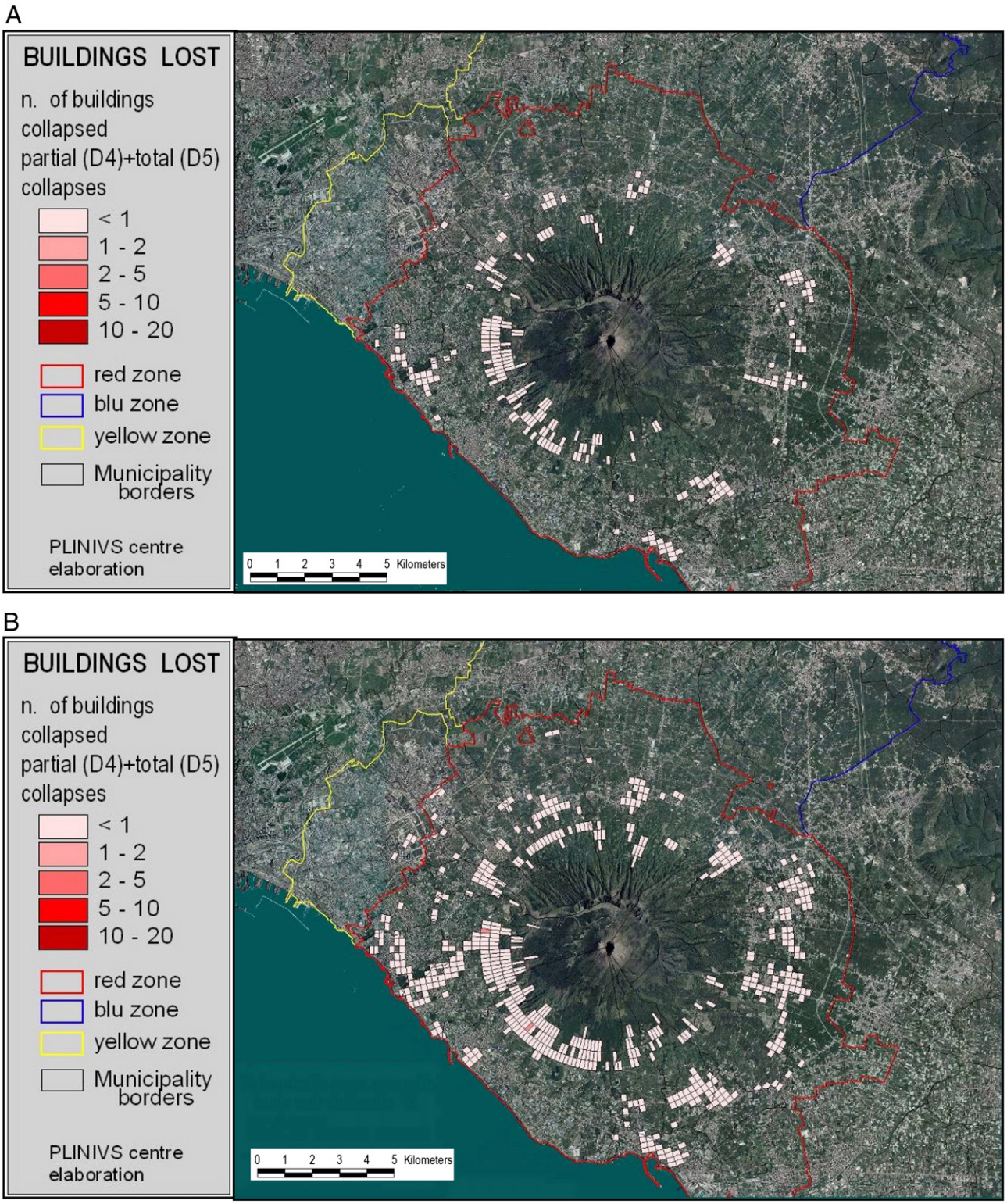

Fig. 30. A. Seismic damage scenario — 1st event: intensity VI. Buildings lost=D4 (partial collapse)+D5 (total collapse). D5=2 buildings. B. Seismic damage scenario — 2nd event: intensity VI. Buildings lost=D4 (partial collapse)+D5 (total collapse). D5=5 buildings. C. Seismic damage scenario — 3rd event: intensity VII. Buildings lost=D4 (partial collapse)+D5 (total collapse). D5=83 buildings. D. Seismic damage scenario — 5th event: intensity VII. Buildings lost=D4 (partial collapse)+D5 (total collapse). D5=231 buildings.

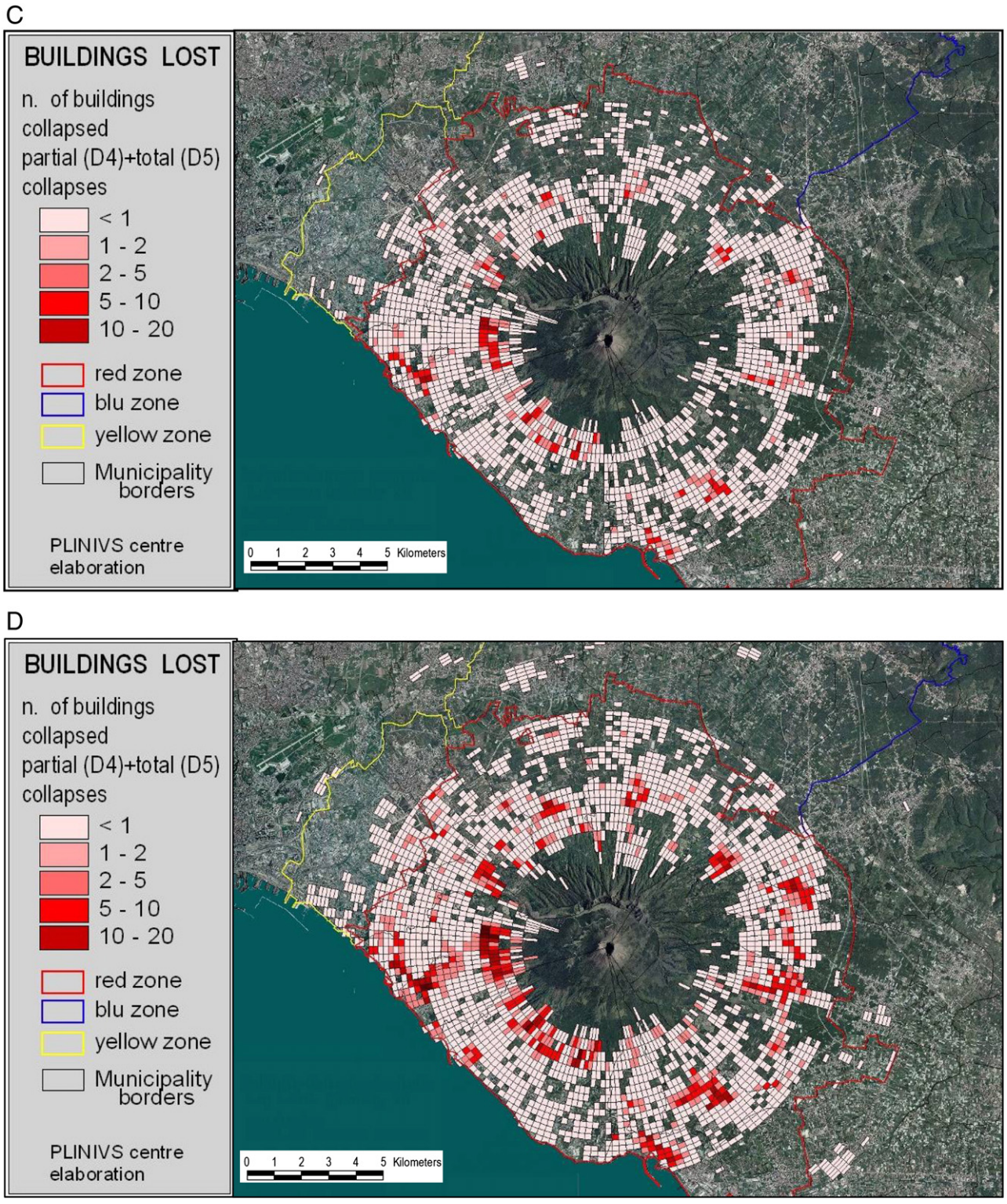

Fig. 30 (*continued*).

phase plan the evacuation of the Red Zone. In Fig. 30 the localization and the quantification of the damage in the cells of the grid are shown. The model allows also to study the possible viability interruption due to total or partial seismic-building collapses, which is a useful tool to suggest the best evacuation paths.

In Table 18 the values of the buildings collapsed are reported.

Table 18
Seismic sequence and relevant cumulative buildings lost (D4+D5) subdivided by each seismic vulnerability class

Events sequence	EQ intensity	A_s	B_s	C_s	D_s	D4	D5	Buildings lost
EQ1	VI	40	4	2	0	44	2	46
EQ2	VI	94	9	6	0	104	5	109
EQ3	VII	692	96	40	1	746	83	829
EQ4	VI	776	109	44	1	840	90	930
EQ5	VII	1589	258	93	2	1711	231	1942

Table 19
Seismic sequence and relevant cumulative casualties

Events sequence	EQ intensity	Population in the area (%)	People killed	People seriously injured	Homeless
EQ1	VI	42	2	6	1208
EQ2	VI	23	4	11	2539
EQ3	VII	16	21	77	12,601
EQ4	VI	9	22	81	14,196
EQ5	VII	2	25	104	25,586

In Table 19 the casualties relevant to the building damages according to the population decay law and the casualty model by Coburn and Spence (2002) are shown.

8.1.2. 2nd Phase

The second phase foresees the starting of the eruption and the consequent ash fallout; a linear law to simulate the increasing of the load on the roofs over time has been assumed. This phenomenon affects consistently either the Red Zone or the Yellow Zone of the Civil Protection Emergency Plan. Therefore the model considers the damage increment on the building roofs of the Red Zone and the damage distribution on the roofs of the Yellow Zone affected by ash fall dispersed in the region by the wind of that day. In Fig. 31 the most probable ash deposit distribution is shown; this input has been computed by numerical simulation (see Macedonio et al., 2005; 2008-this issue for details).

The model computes the cumulative damage on the structures for three intermediate steps of ash deposit at 50% and 75% of the final expected one; then another seismic event of medium intensity (VII), during this phase, is considered. In Fig. 32(A and B) the distributions of the cumulative damage to the buildings in the Red and Yellow Zones for these steps of the sequence are reported.

In Fig. 32C the final damage at the end of the ash fallout phase is shown both for Red and Yellow Zones. In Table 20 the sequence of the events considered in the second phase and the relevant damages scored are reported. In each subsequent table the damage caused by any type of hazard are always referred to the inventory of the seismic-building class typologies.

The failure of the roofs is always considered as D4 (partial collapse), therefore in Table 20 the increment of the value of D5 is always zero except where an earthquake increases the number of the buildings totally collapsed. In the column "buildings lost" the cumulative values of the buildings partially or totally collapsed are shown. It should be noted that the number of

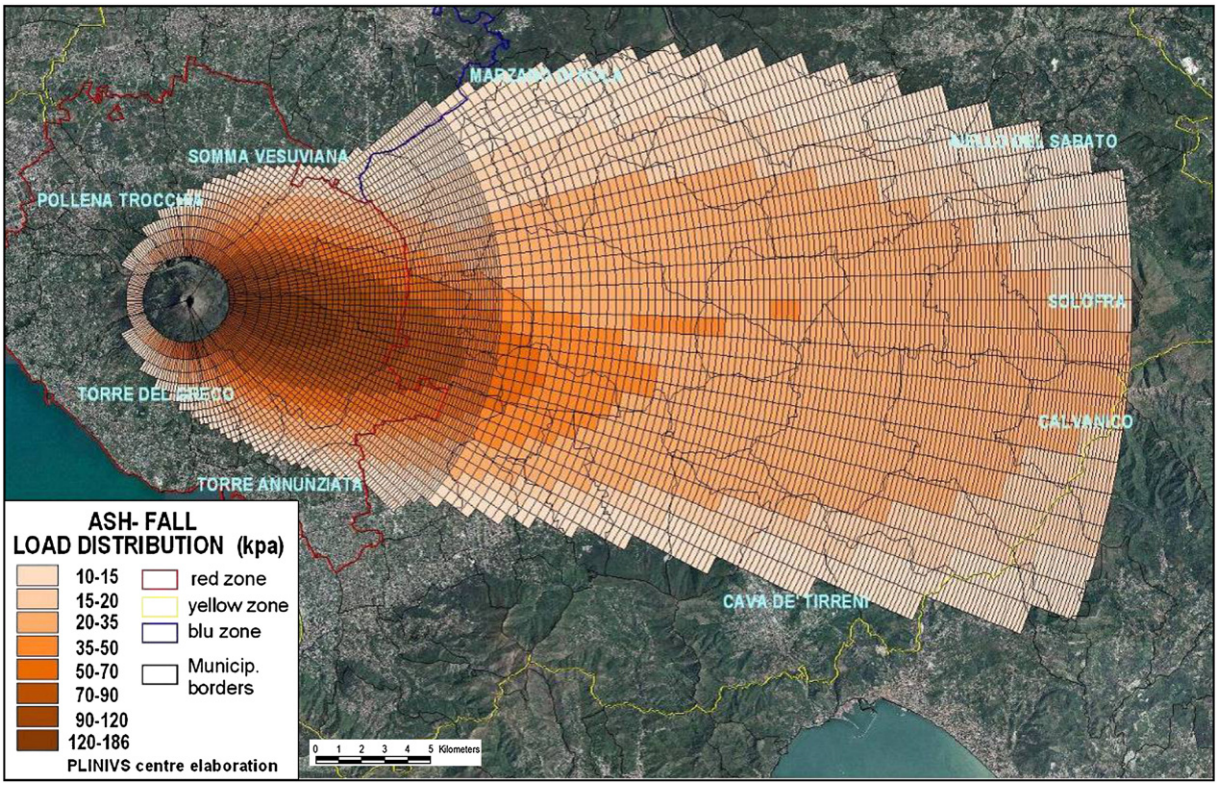

Fig. 31. Ash fall load distribution (Macedonio et al., 2008-this issue).

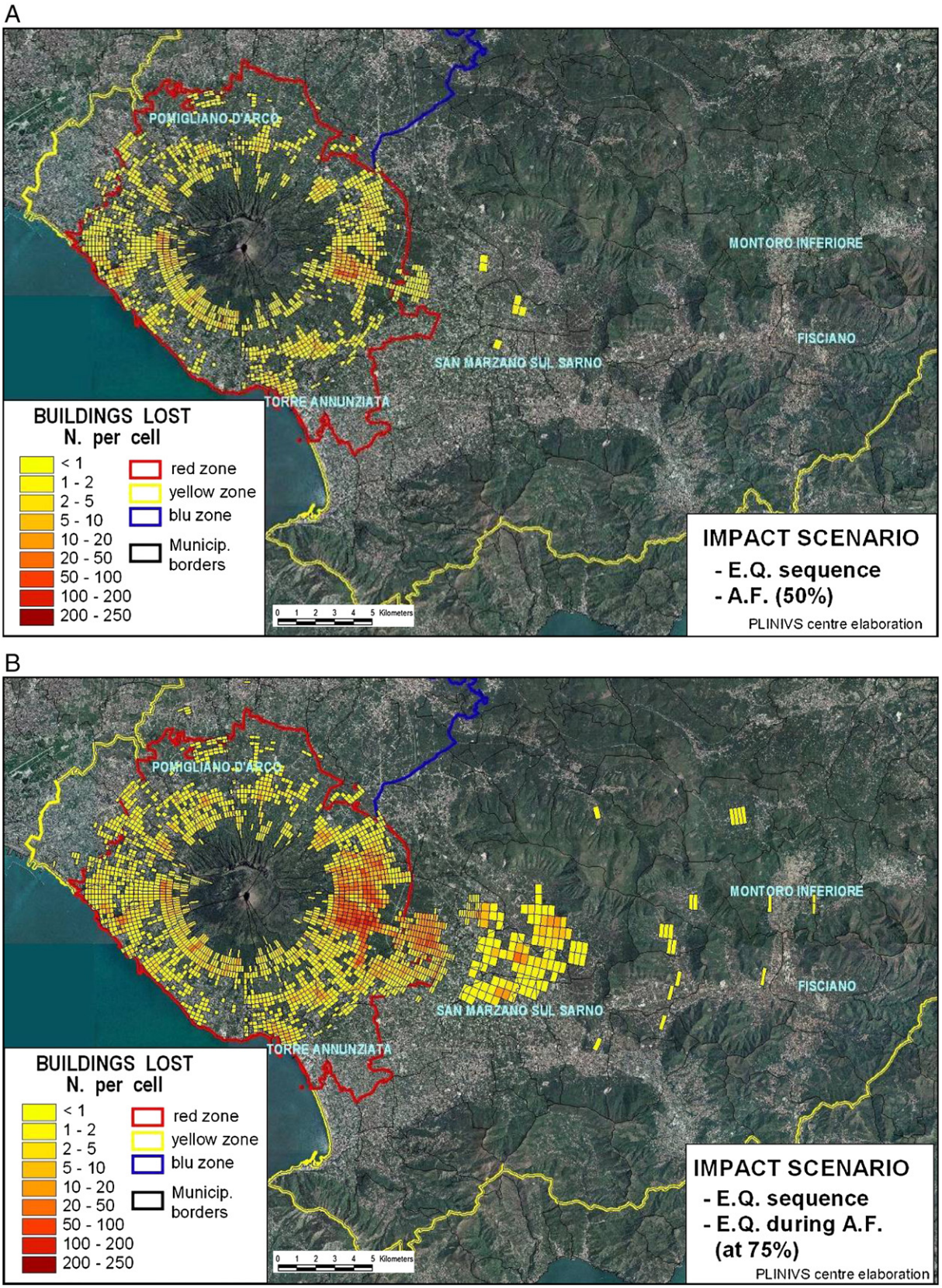

Fig. 32. A. Cumulative building. Damage distribution in the Red Zone at 50% of ash fall load expected. B. Cumulative building. Damage distribution in the Red Zone after a seismic event of intensity VII with 75% of the total ash fall load expected. C. Cumulative building. Damage distribution in the Red and Yellow Zones at 100% of AF phase.

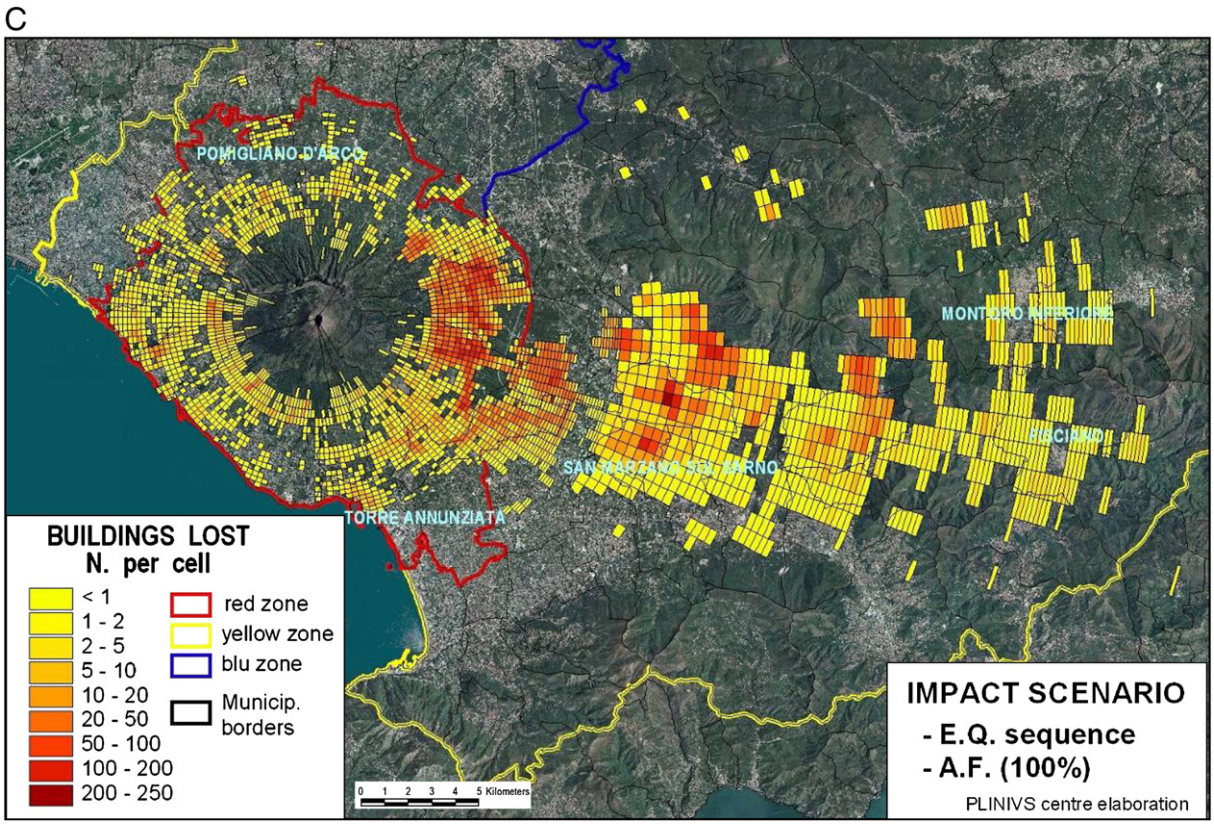

Fig. 32 (*continued*).

killed constitute 1.5% of the total population living in the combined Red and Yellow Zones. The population living in the Red Zone is about 550,000 people while the population staying in the Yellow Zones is about 850,000 people. Considering the limited area involved by the AF in the Yellow Zone, it is evaluated that only 10–15% of the population of this area will participate in the evacuation.

8.1.3. 3rd Phase

The third phase foresees the invasion of the Red Zone by the PFs; this phenomenon, as discussed above, is discrete and randomly distributed on the territory around the Mont Vesuvius. However Neri et al. (2008-this issue) has demonstrated that Sectors A1, A2 and A3 A4 have the highest probabilities to be touched by these ardent currents.

In this application the spatial distribution supplied by the INGV Pisa worst simulation (90% of the mass collapsed) has been assumed. The dynamic pressures and temperatures ranges have been derived from the analyses of the parameters variation performed cell by cell starting from the database of the results provided from INGV Pisa (Neri et al., 2008-this issue).

For each strip of cells along the radial direction from the crater to the runout distance, values of DP and flow temperature T compatible to the decay law supplied by INGV Pisa. Fig. 33 shows the PF simulation assumed as input and the dynamic pressure DP distribution.

In Fig. 34 the cumulative damage distribution after the pyroclastic flow phase is shown.

At first glance comparing the damage map of Fig. 32C at the end of AF phase with the map of Fig. 34 at the end of the PF phase a considerable increment of the damage distribution in the area toward the sea towards the south-west where the PFs mainly are directed in the hazard map can be observed.

In Table 21 the final cumulative damage values are reported.

Another important effect of the pyroclastic flows is the fire ignition. The causes of the building ignition have been studied

Table 20
The ash fall sequence considered and relevant cumulative building damages and casualties

Events sequence	EQ intensity	A_s	B_s	C_s	D_s	D4	D5	Buildings lost	People killed	People injuries	Homeless
AF 25%		1589	258	93	2	1711	231	1942	25	104	25,586
AF 50%		2056	387	138	53	2403	231	2634	149	347	26,864
AF 75%		5187	1940	1381	1726	10,003	231	10,234	1321	2657	48,198
AF 75%+EQ	VII	6090	2132	1438	1728	11,007	381	11,388	1324	3118	59,750
AF 100%		10,909	4532	3496	5576	24,132	381	24,513	5058	10,471	107,886

The values include the damages already done by the EQ sequence.

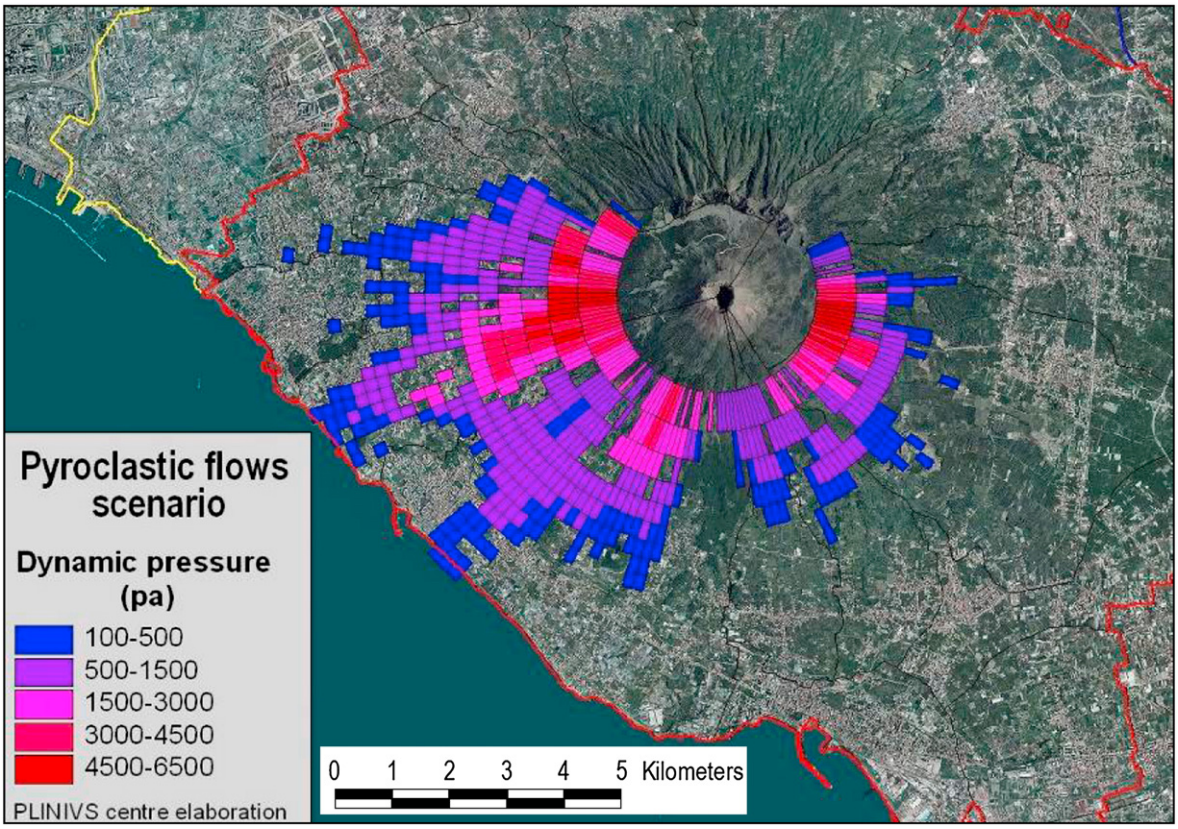

Fig. 33. Assumed PF spatial distribution of the dynamic pressure DP (Neri et al., 2008-this issue).

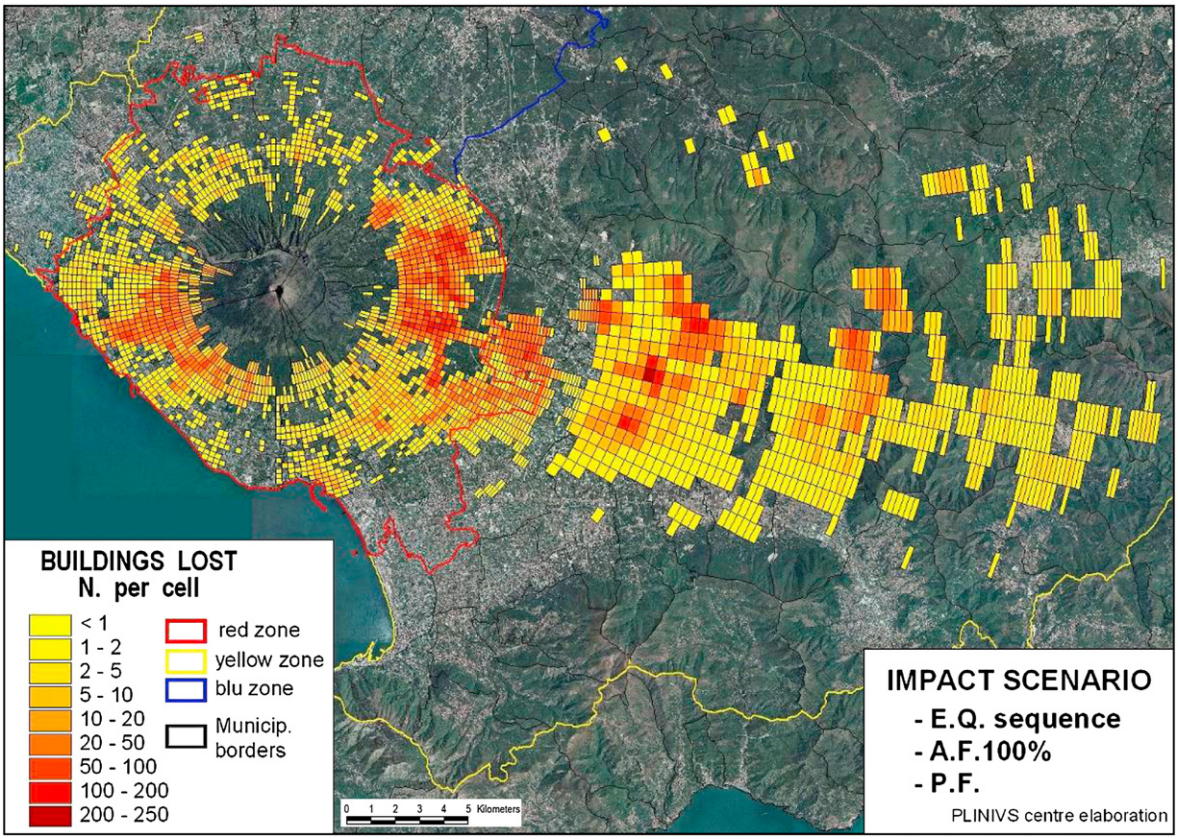

Fig. 34. Final building damage distribution.

Table 21
Final cumulative building damage

Events sequence	A_s	B_s	C_s	D_s	Buildings lost
PF	11,759	4939	4803	7361	28,862

in EXPLORIS and are reported elsewhere (Baxter et al., 2004; Spence et al., 2007).

One of the most important factors influencing this further inducted vulnerability of the building is the resistance of the windows and generally of all the openings to the dynamic pressure. This also influences the survivability of the people trapped in area during this phase; it is described in detail in the casualties model (Spence et al., 2007). From the PF simulations (Neri et al., 2008-this issue) the temperature distribution on the Red Zone can be derived (Fig. 35).

Figs. 36 and 37 show respectively the distribution of the windows failed and of the buildings ignited. The comparison between these two maps shows that the number of buildings which catch fire is considerably smaller than the number of buildings where the windows fail. This is due to the distribution of temperature values, since, according to the studies performed in EXPLORIS (Baxter et al., 2004; Spence et al., 2007) building ignition has been considered only for T greater than 250 °C. The window failure also affects the casualty evaluations.

Table 22 shows the values of the windows failed, the buildings which catch fire and the final value of the cumulative number of buildings lost that is equal to the building damaged by the sequence of the events considered plus the buildings fired.

The final casualty results in Table 23 include either the people involved in the collapse of the buildings or the people involved in other casualty factors such as: high temperature, gas infiltration (due even at windows failure), fire, and the duration of the action of the single pulse on the building that it has been assumed equal to 2 min in this application (Baxter et al., 2004; Spence et al., 2007). The values represent the cumulative impact on the population under the percentage of people in the area assumed for this exercise.

The considerable increment of casualties in this phase is due to traumas for building collapses (397 victims) and to casualties due to high temperature and PF entry or infiltration either in buildings where the windows fail (1553 victims and 1553 injuries) or in buildings where the windows resist (1432 victims and 1432 injuries).

9. Discussion of the results

Table 24 summarises the dynamic growth of the impact reporting step by step each increment of the lost and the

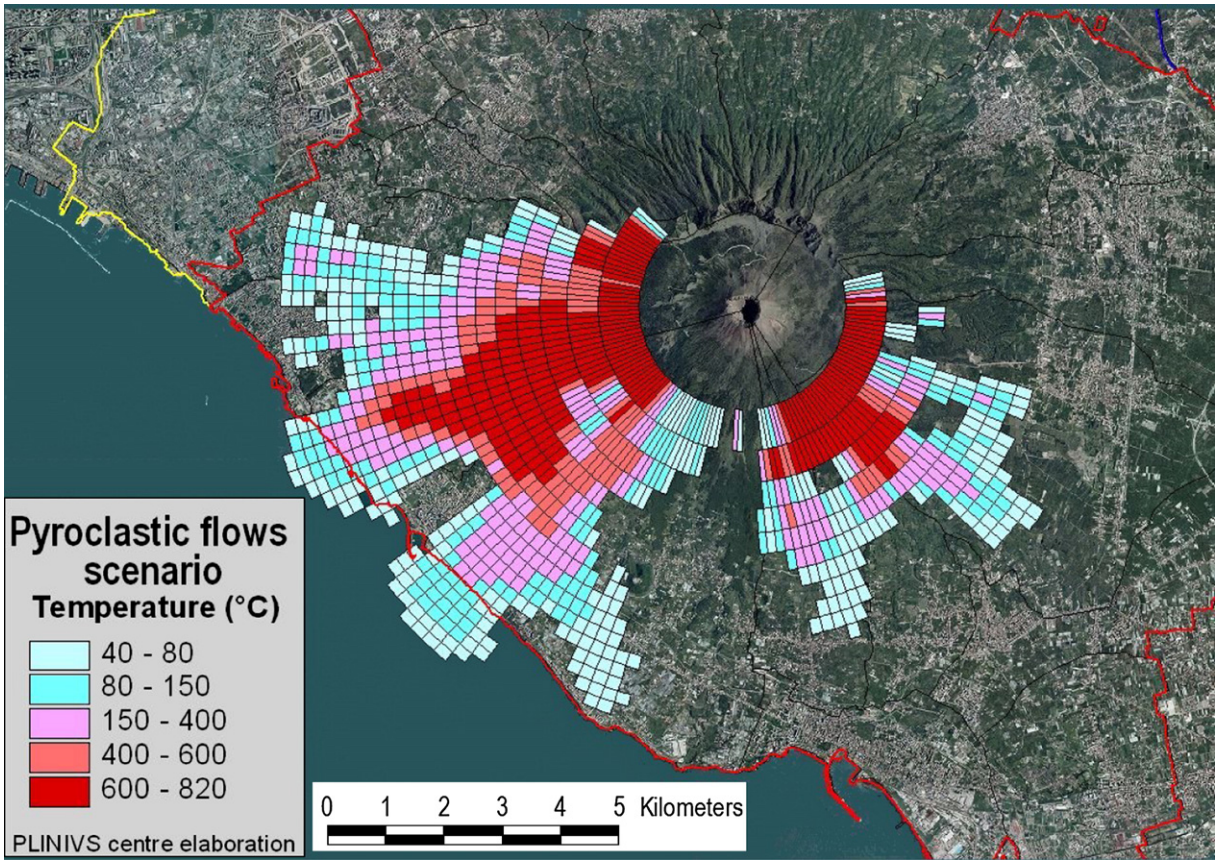

Fig. 35. Temperature distribution consequent to the pyroclastic flow event considered.

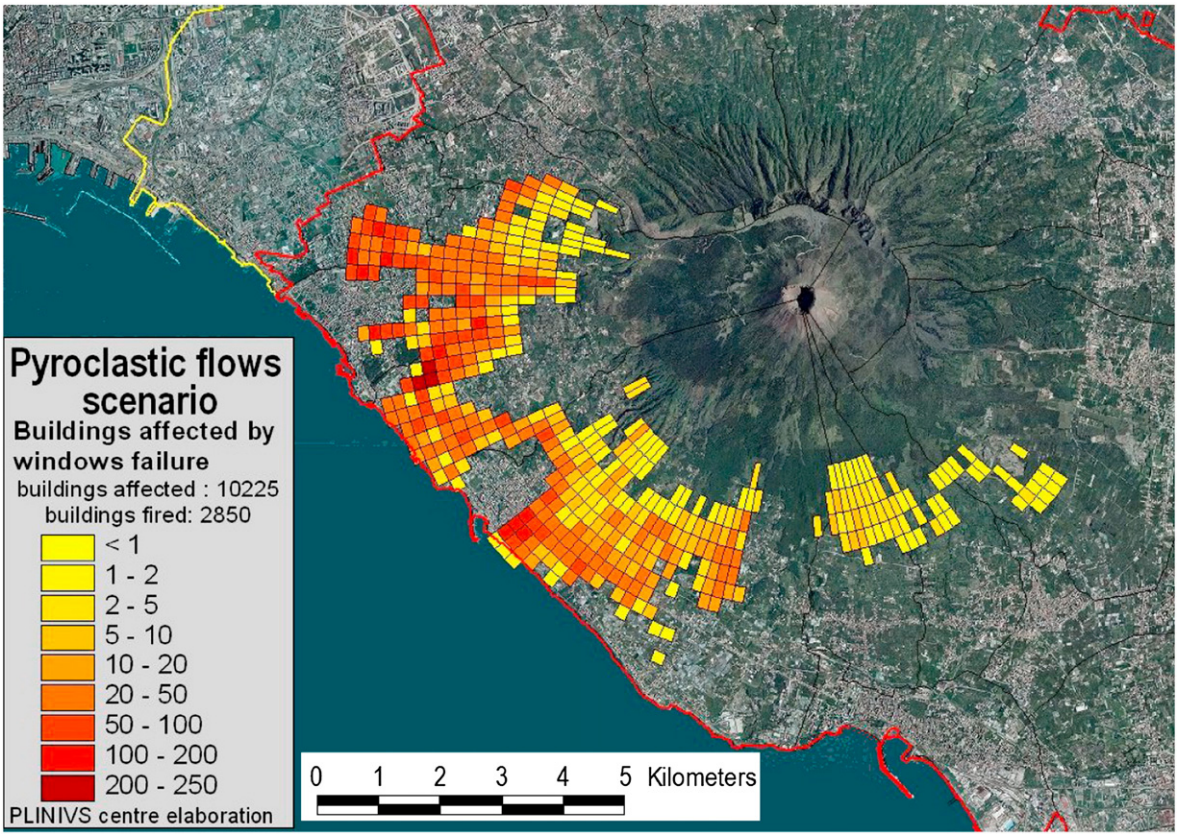

Fig. 36. Window failure distribution consequent to the pyroclastic flow event considered.

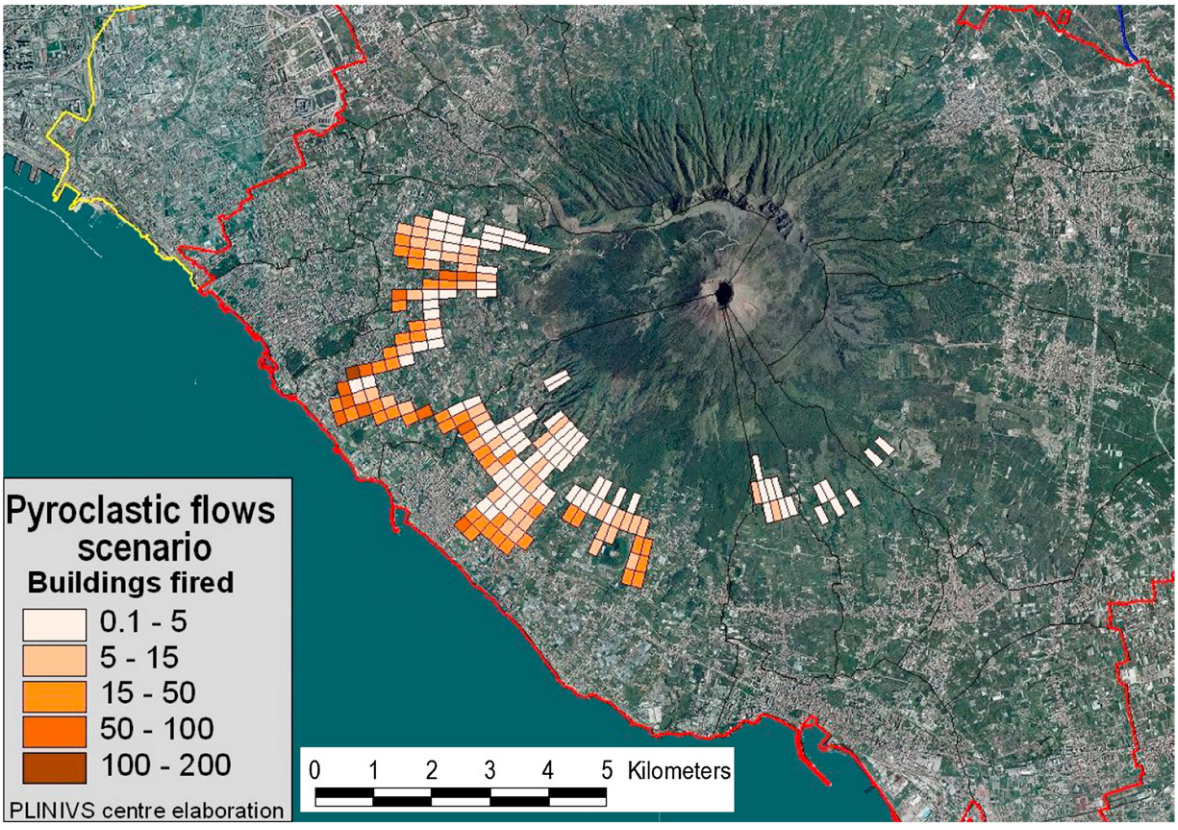

Fig. 37. Buildings which catch fire: distribution consequent to the pyroclastic flow event considered.

Table 22
Windows failed and buildings burned

Events sequence	Buildings lost and burned	Windows failed	Buildings burned	Total buildings lost including fired
PF	28,864	10,225	2850	31,714

The total of "buildings lost" includes only the buildings where the temperature is greater than 250 °C (Baxter et al., 2004; Spence et al., 2007).

Table 23
Final cumulative casualties after the last PF phase

Events sequence	Killed	Injuries	Homeless
PF	8440	13,456	129,581

synthetic cumulative values; from the analysis of the results it can be remarked:

- Considering the numbers of casualties expected assuming that only the 1.5% of the population living in the area is involved in the eruption, the evacuation of all the inhabitants before the eruption is the most important real mitigation measure that the Civil Protection could adopt, and all the efforts to improve the efficiency of the evacuation plan has to be done.
- During the unrest phase a possible earthquake sequence can produce damage to the buildings and to the population. This could interfere with the evacuation activities either for the rescue of people involved or to the interruption of the evacuation viability due to partial or total collapse of same buildings on the roads.
- Assuming the AF phase could last 12 to 18 h the model shows that the main damaging impact on the buildings and the humans still in the area occurs after the 50% of the expected fallout. This circumstance highlights that, although extremely dangerous and not to be included in any kind of Emergency Plan, however the Civil Protection could have at its disposal further few hours after the eruption start to leave the area.
- The most damaging phase of the eruption seems to be for the buildings the second phase (AF), while for the human casualties the second and the third phases, respectively AF and PF share a considerable level of impact.

10. Conclusions

In the paper a first attempt to the development of a probabilistic dynamic model for the volcanic impact evaluation is presented; the work shows the high complexity of the goal and traces a possible path to pursue it.

The most relevant difficulties identified are:

- the unpredictability of the input, in particular of the number and intensity of the phenomena distributed along the time history expected for a given eruptive scenario (Sub-Plinian I as studied in the paper);
- the considerable uncertainty in the evaluation of the cumulative damage on the building typologies and in the graduation of the damage levels attributed by the combined vulnerability functions for each event;
- the incompleteness of the building and infrastructure inventory data;
- the time of computing to converge at the solution in the "Random Mode".

On the other hand the positive features of the model are:

- the dynamic control of the damage distribution evolving in time and space,
- the unexplored field of applications of the results aroused during a recent exercise of evacuation led by the Italian Civil Protection where the impact scenarios traced by this model in real time along the simulated emergency has opened for several of the actors involved in the crisis new perspectives of work and planning (i.e. providers of telecommunication, water and gas, transportation network availability etc.),
- great potential for improvement considering:
  - the number of the input variables involved on which the knowledge are still limited and highly uncertain

Table 24
The dynamic growing of the impact

Events	Buildings lost (D4+D5+burned)				Casualties				
Sequence	By step	Cumulative	Burned	Total	Population in the area (%)	Killed by step	Killed (cumulative)	Injuries by step	Injuries cumulative
EQ1 (VI)	46	46	0	0	42	2	2	6	6
EQ2 (VI)	63	109	0	0	23	2	4	5	11
EQ3 (VII)	720	829	0	0	16	17	21	66	77
EQ4 (VI)	101	930	0	0	9	1	22	4	81
EQ5 (VII)	1012	1942	0	0	2	3	25	23	104
AF 25%	0	1942	0	0	1.5	0	25	0	104
AF 50%	692	2634	0	0	1.5	124	149	243	347
AF 75%	7600	10,234	0	0	1.5	1172	1321	2310	2657
AF 75%+EQ (VII)	1154	11,388	0	0	1.5	3	1324	461	3118
AF 100%	13,125	24,513	0	0	1.5	3734	5058	7353	10,471
PF	4351	28,864	2850	31,714	1.5	3382	8440	2985	13,456

The increment of the damage is step by step and cumulative.

  - the almost unexplored field of volcanic engineering for single and combined phenomenon actions
  - the pioneering level of the computerised prototype of the model
  - the high but not exhaustive knowledge of the structural and infrastructural inventory
  - the possibility to investigate the calibration of the model on the basis of data available from past eruptions.
- the capability to perform sensitivity analyses to focus either the reliability of some assumptions done in the process or to evaluate the importance of the single parts of the model for different applications,
- to supply a tool to the Italian Civil Protection useful to develop scenarios on the basis of which planning the Emergency Plan and possible Mitigation Measures can be carried out.

Further improvements of the results could be achieved either by refinement on the understanding of the physics of the eruptive process or by refinements of the vulnerability functions available at the moment. The growth of the knowledge on the characteristics of the buildings and infrastructures in the area, and the improvement potential of the numerical elaborations either regarding the AF and PF simulations or the impact model itself, will allow to have at disposal a more efficient and reliable tool for the Civil Protection. The hope is that the effort of EXPLORIS Project might help the people, institutions and all the subjects involved in one of the most tremendous disaster expected in the world.

Acknowledgements

The EU-funded EXPLORIS Project (EVR1-CT-2002-40026) supported this work involving many tens of scientists in several countries: we gratefully acknowledge all their contributions to the work reported here. Partial support was also provided by the Dipartimento di Protezione Civile, Italy; special thanks to Bernardo De Bernardinis and Franco Barberi for their suggestions, remarks and encouragements.

References

Aspinall, W.P., 2006. Structured elicitation of expert judgment for probabilistic hazard and risk assessment in volcanic eruptions. In: Mader, H.M., Coles, S.G., Connor, C.B., Connor, L.J. (Eds.), Statistics in Volcanology. Geological Society of London, pp. 15–30. on behalf of IAVCEI.

Aspinall, W., Baxter, P., Bertagnini, A., Cioni, R., Cole, P., Hincks, T., Neri, A., Zuccaro, G., 2008-this issue. Event tree and probabilistic risk assessment at Vesuvius.

Baratta, A., Zuccaro, G., 1989. Valutazione Preliminare di Rischio Sismico per gli Insediamenti Urbani (Il Centro Storico di Napoli) - Atti del "4° Convegno Nazionale - L'ingegneria Sismica In Italia", Milano.

Baratta, A., Zuccaro, G., Binetti, A., 2004. Strength capacity of No Tension portal arch-frame under combined seismic and ash loads. J. Volcanol. Geotherm. Res. 133, 369–376.

Barsotti, S., Neri, A., in press. The VOL–CALPUFF model for atmospheric ash dispersal. II. Application to the weak Etna plume of July 2001, Journal of Geophysical Research.

Barsotti, S., Neri, A., Scire, J., in press. The VOL–CALPUFF model for atmospheric ash dispersal. I. Approach and physical formulation, Journal of Geophysical Research.

Baxter, P.J., 1990. Medical effects of volcanic eruptions; I—main causes of death and injury. Bull. Volcanol. 52 (7), 532–544.

Baxter, P.J., Neri, A., Todesco, M., 1998. Physical modelling and human survival in pyroclastic flows. Nat. Hazards 17, 163–176.

Baxter, P.J., Spence, R.J.S., Zuccaro, G., 2004. Building vulnerability and human casualty estimation for a pyroclastic flow: a model and its application to Vesuvius. J. Volcanol. Geotherm. Res.

Baxter, P.J., Cole, P.D., Spence, R., Zuccaro, G., Boyd, R., Neri, A., 2005. The impacts of pyroclastic density currents on buildings during the eruption of the Soufrière hills volcano, Montserrat. Bull. Volcanol. vol. 67, 292–313.

Baxter, P., Spence, R., Zuccaro, G. 2008-this issue. Risk mitigation and emergency measures at Vesuvius.

Braga, F., Dolce, M., Liberatore, D., 1982. A statistical study on damaged buildings and ensuing review of MSK-76 scale, Southern Italy November 23 1980 Earthquake. Progetto Finalizzato di Geodinamica, CNR Italia, Pub. No. 503 (7ECEE, Athens). Edizioni Scientifiche Associate, Roma.

Carafa, G., 1632. In opusculum de novissima Vesuvij conflagratione, epistola isagogica, 2ª ed. European Geosciences Union, Napoli, Naples.

Cherubini, A., Petrazzuoli, S., Zuccaro, G., 2002. Vulnerabilità Sismica dell'Area Vesuviana. Giannini Ed., Roma.

Cosenza, E., Manfredi, G., Verderame, G., 2000. Seismic assessment of r.c. structures: case studies in Catania. In: Faccioli, E., Pessina, V. (Eds.), The Catania Project: Earthquake Damage Scenario for a High Risk Area in the Mediterranean. Gruppo Nazionale per la Difesa dai Terremoti. CNR, Roma. 215 pp.

Costa, A., Macedonio, G., Folch, A., 2006. A three-dimensional Eulerian model for transport and deposition of volcanic ashes. Earth Planet. Sci. Lett. 241, 634–647.

Coburn, A.W., Spence, R., 2002. Earthquake Protection, 2nd ed. John Wiley, pp. 338–342.

Dai, H., Xia, L.P., Ding, Y.Z., 1996. Aseismic construction for multi-storey composite structures. Earthq. Eng. Struct. Dyn. 25, 87–907.

Del Pezzo, E., Zollo, A., 2005. Report of the working group on Seismic scenarios at Vesuvius and Campi Flegrei volcanic areas. Maximum Earthquake Expected at Vesuvius and Campi Flegrei. Italian Dep. of Civil Protection.

Di Pasquale, G., Orsini, G., 1997. Proposta per la valutazione di scenari di danno conseguenti ad un evento sismico a partire dai dati ISTAT, Atti 8° Convegno Nazionale ANIDIS, L'ingegneria Sismica in Italia, Taormina: 477–486.

Department of Civil Protection, 2001. Piano Nazionale di Emergenza dell'Area Vesuviana. Presidenza del Consiglio dei Ministri, Governo Italiano, Roma.

Department of Civil Protection, 2006. Report of Working Group on Volcanic Seismic Scenarios Del Pezzo E., Zollo A.

EMS '98 — European Macroseismic Scale, 1998. Conseil de l'Europe — European Seismological Commission — 8 LUXEMBOURG 1998.

Grimaz, S., Meroni, F., Petrini, V., Tomasoni, R., Zonno, G.,1997. Progressi nel settore della vulnerabilità sismica degli edifici in muratura derivanti dall'analisi dei dati di danneggiamento del terremoto del Friuli, La scienza e i terremoti - Analisi e prospettive dall'esperienza del Friuli - 1976/1996, 14–16 Novembre 1996, Udine, Forum ed. Udine, pp. 89–96.

Guidoboni, E., 2008-this issue. An historical approach to the 1631 Vesuvius eruption: analysis of three contemporary treatises: results and some prospects.

Gutenberg, B., Richter, C.F., 1956. Earthquake magnitude, intensity, energy and acceleration (second paper). Bull. Seismol. Soc. Am. 40, 105–145.

Kalnay, E., Kanamitsu, M., Kistler, R., Collins, W., Deaven, D., Gandin, L., Iredell, M., Saha, S., White, G., Woolen, J., Zhu, Y., Chelliah, M., Ebisuzaki, W., Higgins, W., Janowiak, J., Mo, K.C., Ropelewski, C., Wang, J., Leetmaa, A., Reynolds, R., Jenne, R., Joseph, D., 1996. The NCEP/NCAR 40-year reanalysis project. Bull. Am. Meteorol. Soc. 77, 437–470.

Macedonio, G., Costa, A., Longo, A., 2005. HAZMAP: a computer model for volcanic ash fallout and assessment of subsequent hazard. Comput. Geosci. 31, 837–845.

Macedonio, G., Costa, A., Folch, A., 2008-this issue. Ash fallout scenarios at Vesuvius: numerical simulations and hazard assessment implications. J. Volcanol. Geotherm.

Mascolo, G.B., 1634. De incendio Vesuvii excitato xvij. Kal. Ianuar. anno trigesimo primo sæculi Decimiseptimi libri X. Cum Chronologia superiorum

incendiorum; & Ephemeride ultimi. European Geosciences Union, Napoli, Naples.
Meli, R., 1991. Code prescribed seismic action and actual seismic forces in buildings. Proc. 5th National Conference L'Ingegneria Sismica in Italia, Milan, pp. 735–758.
Neri, A., Esposti Ongaro, T., Macedonio, G., Gidaspow, D., 2003. Multiparticle simulation of collapsing volcanic columns and pyroclastic flows. J. Geophys. Res. Lett. 108, 2202. doi:10.1029/2001 JB000508.
Neri, A., Esposti Ongaro, T., Menconi, G., Cavazzoni, C., Erbacci, G., 2008-this issue. 3D Numerical simulation of pyroclastic flow scenarios at Vesuvius.
Pomonis, A., Spence, R., Baxter, P., 1999. Risk assessment of residential buildings for an eruption of Furnas Volcano, Sao Miguel, the Azores. J. Volcanol. Geotherm. Res. 92, 107–131.
Spence, R., Pomonis, A., Baxter, P., Coburn, A., 1997. Building damage caused by the Mount Pinatubo eruption of June 15th, 1991. In: Newhall, C.G., Punongbayan, R.S. (Eds.), Fire and Mud: Eruptions and Lahars of Mt Pinatubo, Philippines. Washington University Press, pp. 1005–1012.
Spence, R., Brichieri-Colombi, N., Holdsworth, F., Baxter, P., Zuccaro, G., 2004a. Vesuvius: building vulnerability and human casualty estimation for a pyroclastic flow (25 pages). J. Volcanol. Geotherm. Res.133, 321−343. ISSN: 0377-0273.
Spence, R., Zuccaro, G., Petrazzuoli, S., Baxter, P.J., 2004b. The resistance of buildings to pyroclastic flows: theoretical and experimental studies in relation to Vesuvius. ASCE Nat. Hazards Rev. 5,48−50. ISSN: 1527-6988.
Spence, R., Kelman, I., Petrazzuoli, S., Zuccaro, G., 2005. Residential Buildings and Occupant Vulnerability to Tephra Fall. Nat. Hazards Earth Syst. Sci. European Geosciences Union, pp. 1–18.
Spence, R., Kelman, I., Brown, A., Toyos, G., Purser, D., Baxter, P., 2007. Residential building and occupant vulnerability to pyroclastic density currents in explosive eruptions. Nat. Hazards Earth Syst. Sci. 7, 219–230.
Varrone, S., 1634. Vesuviani incendii historiae libri tres. European Geosciences Union, Napoli, Naples.
Woo, G., 1999. The Mathematics of Natural Catastrophes. Imperial College Press, London.
Zuccaro, G., 2000. Structural vulnerability to possible flows consequent to the eruption of the volcano Vesuvius. Final Report for EC Project ENV4-CT98-0699, Laboratorio di Urbanistica e Pianificazione Territoriale. University of Naples.
Zuccaro, G., 2004. Final Report SAVE. Project Link to the Web Page of the "Save" Project in "Atlantis". http://gndt.ingv.it/Att_scient/Prodotti_attesi_2004/Dolce_Zuccaro/Mappe/Start2.htm. Roma.
Zuccaro, G., submitted for publication. Structural vulnerability functions in volcanic engineering. ASCE Natural Hazards Review.
Zuccaro, G., Baratta, A., 1999. Valutazione di Base del Patrimonio Edilizio Nazionale. Rapporto Finale. Convenzione SSN–Centro LUPT Università di Napoli.
Zuccaro, G., Petrazzuoli, S.M., 2004a. Structural resistance of RC buildings under pyroclastic flows: a study on the Vesuvian area. J. Volcanol. Geotherm. Res. 133, 353–367.
Zuccaro, G., Ianniello, D., 2004b. Interaction between pyroclastic flow and the building structures of an urban settlement. A fluid-dynamic simulation impact model. J. Volcanol. Geotherm. Res 133, 345–352.
Zuccaro, G., Cacace, F., 2006. In: PATRON (Ed.), Procedura di valutazione speditiva della vulnerabilità per gli edifici strategici della Regione Campania. J. Ing. Sism. vol. 2, vol. 2.
Zuccaro, G., Cacace, F., 2007a. Le nuove mappe di rischio sismico a scala nazionale. Proc. ANIDIS, Pisa.
Zuccaro, G., Cacace, F., 2007b. A probabilistic model for the evaluation of the impact of explosive eruption scenarios at Vesuvius. International Symposium on Recent Advances in Mechanics, Dynamical Systems and Probability Theory — MDP-2007 — Palermo, June 3–6.
Zuccaro, G., Della Bella, M., Papa, F., 1999. Caratterizzazione tipologico strutturali a scala nazionale. Atti 9° Convegno Nazionale ANIDIS, L'ingegneria Sismica in Italia, Torino.